

Final Report
for the
Task A11 -
Part 107 Waiver Request Case Study



Rotorcraft Systems Engineering and Simulation Center

Contract Number: 15-C-UAS-UAH-02

PoP: 8/4/2015 to 9/30/2016

Mr. David Arterburn, Principal Investigator

UAH Contract Title: F/FAA/Part 107 Waiver Request Case Study

UAH Org: 675418

Contents

List of Figures	3
List of Tables	4
Executive Summary	5
1. Introduction	6
1.1. Background	6
1.2. Scope	6
1.3. Relationship to Research conducted by ASSURE Project A4	7
1.4. Final Report Organization	7
2. Details of Testing and Analysis Conducted to Develop Height-Velocity Limits	8
2.1. Overview of Approach for Developing Height-Velocity Limits	8
2.2. Ballistic Modeling and CFD Analysis	8
2.3. Flight Testing	9
2.4. NIAR Drop Testing	11
2.5. Energy Transfer Analysis	25
2.6. Pendulum Testing of Blade Guards as a Laceration Mitigation	33
3. Proposed Standards	38
4. Conclusion and Recommendations	39
5. Future Research Proposed to Address Research Gaps	40
5.1. Dynamic Modeling of UAS for a Wider Variety of Failure Modes	40
5.2. Blade Guard Development and Standards	40
5.3. Parachute Standards to Reduce Impact KEs	40
5.4. Probability of Ground Collision with People	41
5.5. Additional sUAS Collision Tests and Development of an FMVSS 208 Like Analytical Standard	41
Appendix A – UAH Part 107 Waiver Submission for Flight Over People	A-1
Appendix B - NIAR Test Article Damage	B-1
Appendix C - Proposed Standard with Impact KE Assessment Only	C-1
Appendix D - Proposed Standard with Evaluation of Potential Injury Severity	D-1

List of Figures

Figure 1 - Comparison of Simulation and Flight Test Results	11
Figure 2 - Top View of Sled Setup for UAS Drop	13
Figure 3 - Front Left View of Sled Setup (upper left), Vertical Drop Position of Dummy and UAS (upper right), Pendulum Setup for Horizontal Impact Test (lower left), and Dummy and UAS Setup for Angle Impact Test (lower right).....	14
Figure 4 - Example NIAR Test Summary for an Individual Test.....	15
Figure 5 - Example NIAR Time History for an Individual Test.....	16
Figure 6 - Probability of Fatality from Debris Impacts for Various Body Parts from RCC 321-00	18
Figure 7 - Probability of Fatality from Debris Impacts for Various Body Positions.....	19
Figure 8 - Average Probability of Fatality from Debris Impacts.....	19
Figure 9 - Analysis of Resultant Impact for Skull Fractures versus Impact KE.....	22
Figure 10 - Probability of Neck Injury Trends from NIAR Test Data	23
Figure 11 - Phantom 3 Advanced Waiver Request Envelope.....	24
Figure 12 Time History of Upper Neck Z-direction Force During a NIAR Drop Test.....	27
Figure 13 - Modified blade guard link (highlighted with red oval).....	34
Figure 14 - Blade guard impact test.....	35
Figure 15 - Visual Marker Configuration During Tests 8 and 9.....	35
Figure 16 - Guard Damage during test 8 (left) and test 9 (right).....	36
Figure 17 - Force Components on Blade Guard at 55 deg Impact Angle.....	37
Figure 18 - Static Load Testing Showing Blade Guard Contact with the Blade Under 1kg Loading (contact is show in red oval).....	38
Figure B - 1 - Buckling on Test Article UA17A-05	B-2
Figure B - 2 - Internal Fuselage Cracking on Test Article UA17A-24	B-3
Figure B - 3 - Significant Buckling and Cracking on Fuselage of Test Article UA17A-11.....	B-3
Figure B - 4 - Bent propeller on the Test Article UA17A-13.....	B-4
Figure B - 5 - Damage on Payload Base Plate on Test Article UA17A-11	B-4
Figure B - 6 - Camera Separation from Gimbal at the Elevation Motor on Test Article UA17A-10.....	B-5
Figure B - 7 - Complete Payload Separation in Test Article UA17A-22	B-5
Figure C-1 - Testing and Analysis Standard Block Diagram	C-2
Figure D-1 - Testing and Analysis Flow Chart and Data Input Requirements.....	D-2

List of Tables

Table 1 - UAS Drop Testing Summary	13
Table 2 - NIAR Instrumentation for UAS Drop Tests.....	15
Table 3 - NIAR Summary Test Results and Injury Metrics	17
Table 4 - Difference in Injury Metrics Between FMVSS 208 and RCC Standards	1
Table 5 - Injury Characteristics for Some Common Objects.....	17
Table 6 - Resultant Head Forces from NIAR Tests.....	18
Table 7 –Biomechanical Data for All Skull Fractures from Gurdjian.....	20
Table 8 –Biomechanical Data of Skull Fracture Tests using a 48mm radius Hydraulic Anvil....	20
Table 9 - Comparison of RCC Standards vs. Modified Impact Energy Thresholds for Various Aircraft Weights when Descending under Parachute.	25
Table 10 - Differences in Impact KE and Energy Transferred to ATD Head	29
Table 11 - Impact Energy Absorption by the ATD Dummy Head and Injury Metrics	31
Table 12 - UAS Impact KE and Post-Impact KE from Photometric Data	33
Table 13 - Pendulum Test Results	36
Table B - 1 Summary of Test Article Damage	B-1
Table C-1 - SSL Properties for CFD Analysis.....	C-5
Table C-2 - Flight Test Instrumentation Requirements	C-7
Table D-1 - SSL Air Properties for CFD Analysis	D-5
Table D-2 - Flight Test Instrumentation Requirements	D-7

Executive Summary

The FAA requested research to explore the data requirements and analysis needed to submit a Part 107 waiver for flight over people. The submission of the waiver in conjunction with the research allowed the team to exercise the approval process and define standards that might be used to improve the waiver process for more challenging waivers such as operations meeting the Category 3 and 4 Performance Standards defined by the Micro-ARC Final Report. The research led to successful submission of a Part 107 waiver for flight over people for the Phantom 3 Standard and Advanced, including substantiation data to meet the Category 4 Performance Standards defined by the Micro-ARC Final Report¹. The waiver and this final report include new methodologies for determining safety thresholds other than those used by the Range Commanders Council (RCC). The new 98% confidence level resultant load factor threshold in Appendix D is based upon test data from aircraft drops onto a crash test dummy, skull fracture testing, and other references used to establish similar collision metrics. The new standard applies to multi-rotors in this Phantom 3 class of vehicles since their collision dynamics and collision geometries are dramatically different than small mass, large volume, metallic debris fragments that served as the basis for Probability of Fatality (PoF) charts developed as part of the RCC's assessment of range safety for hypervelocity projectiles and missiles. Flexible, plastic vehicle structures and frangible payloads do not transfer energy during collisions in the same manner as the smaller metal debris used as the basis for RCC standards. The structure, landing gear and blade guards serve as flexible, compliant barriers that minimize the absorption of energy by the body, reduce the possibility of collision with the center of mass of the vehicle and minimize collision impacts with smaller areas of the body such as the thorax. The focus of the analysis addresses skull fractures and injury to the neck area since these are the most vulnerable areas when operating over people, especially under the operating conditions required to meet the Category 4 Performance Standards. The modification of impact energy standards from the RCC standards is a new approach and provides better insight into the injury mechanisms associated with sUAS ground collisions with humans. Safe operation can be conducted when operating these sUAS platforms over people, and the application of the KE standards in this report extends the capabilities of safety mechanisms such as parachutes for larger platforms up to 25.4 lbs for flight over people under Category 4 Performance Standards.

Many of these approaches are new for UAS applications, but they originate from well-established research areas. The methods proposed in this research provide an initial framework for clear standards for evaluating commercial platforms for future waivers required for flight over people as outlined in Appendix C and D. Laceration injuries due to blades and penetration injuries must always be addressed by the applicant, and an operational risk assessment must be completed to evaluate all the hazards and impacts that may affect safe operations when flying over people. The waiver request submitted in Appendix A provides a framework for such an assessment for flight over people.

1. Introduction

1.1. Background

This research seeks to develop and validate a technical approach for Concept of Operations (CONOPS) analysis, risk mitigation, and experimental validation of hazard controls for successful submission of a waiver to Part 107 restrictions on sUAS operations over people. The safety case and subsequent waiver language included mitigations necessary for the waiver depending on the level of safety required by the FAA for flight over people. Per the Micro Unmanned Aircraft Systems (UAS) Aviation Rulemaking Committee (ARC) Recommendations and Final Report¹, flight “over people” is defined as UAS flight directly above one or more persons.

This research included three parallel efforts. The first was a modeling effort underpinned by developing risk and scenario-based area weighted, impact kinetic energy (KE) thresholds by way of CONOPS analysis, determination of operationally appropriate technical data requirements, test and analysis requirements, and the development of suitable operational envelopes developed around injury potential and the associated impact KE. These thresholds, in conjunction with vehicle parameters (weight, effective areas, drag coefficients, and impact energy absorption) and ballistic models, were used to calculate an operating height-velocity diagram to ensure that vehicles do not exceed the impact KE thresholds. The second effort is verification of model inputs and outputs by way of flight and drop tests. The final effort is to develop a set of mitigations to keep the aircraft within the impact KE thresholds and/or to limit the potential of laceration and penetration injuries following blade or UAS body impacts and submit a request for waiver for a single sUAS.

1.2. Scope

The following research questions were addressed by this research:

1. What are the technical data requirements, test and analysis requirements, and suitable operational envelopes necessary or suitable for small unmanned aircraft operations over people based on operational missions/areas covered by the waiver request?
2. What are suitable impact KE thresholds based on the Micro ARC Report's recommendations and what operational limitations and other mitigations are required based upon the impact energy thresholds to achieve the operational requirement?
3. What percentage of vehicle impact KE is absorbed by a person on impact?
4. What are the vehicle height-velocity combinations that ensure vehicles remain below impact KE limits with and without mitigations?

¹ Micro Unmanned Aircraft Systems Aviation Rulemaking Committee (ARC), *ARC Recommendations Final Report*, April 1, 2016

5. What are effective mitigations to reduce the severity of penetration injuries and laceration injuries to reduce collision severity for sUAS operations over people for the proposed scenarios?

1.3. Relationship to Research conducted by ASSURE Project A4.

This research is being conducted in parallel with A4, “Ground Collision Severity Evaluation”, but with a later starting date for the period of performance. The requested start date for this proposal, July 20, 2016, allows research results from A4 to support this proposed research. Research performers from A3 and A4 also support this proposed work to enhance coordination.

The methods and tools being utilized for this research build upon those established in the UAS Characteristics White Paper submitted as part of the A4 Ground Collision Severity Project and impact testing methods employed by the A3 Air Collision Severity Evaluation Project.

This report informs changes in methodologies and results from those developed in Task A4 based upon test results, and it provides an evolution of knowledge developed during the A4 work prior to the execution of this task. The Task A4 Final Report will leverage data collected under the A11 Task and utilize the knowledge that has been gained, in particular the relationship of Abbreviated Injury Scale (AIS) injury metrics and impact KE. This work provides information that is more relevant to sUAS impacts than the RCC Probability of Fatality (PoF) metrics derived from debris and non-lethal munition research that informed much of the Task A4 work to this point.

1.4. Final Report Organization

Appendix A – UAH Part 107 Waiver Submission for Flight Over People contains the Part 107 Waiver Request² for flight over people with a Phantom 3 Standard and a Phantom 3 Advanced submitted to the FAA that was prepared under this task. Data included in Appendix A, B and C of the Part 107 Waiver Request will be referenced in this final report but will not explicitly be replicated. Paragraph 2 will address technical details of the analysis and testing that was not included in the waiver request, Paragraph 3 will address a proposed standard for testing future vehicles to meet the Category 4 Performance Standards outlined in the Micro Unmanned Aircraft Systems Aviation Rulemaking Committee (Micro-ARC) Recommendations Final Report dated 1 April 2016. Paragraph 5 will address research gaps identified during this research effort.

² Part 107 Waiver request to § 107.39 Operation Over Human Beings for the Phantom 3 Standard and Phantom 3 Advanced by the University of Alabama in Huntsville to support research activities as well as collect video images for use in documenting university events. The waiver request includes data and technical evaluations to substantiate safe limits for the Phantom 3 Standard and Advanced aircraft operating over people that meet the Category 4 Performance Standards outlined in the Micro Unmanned Aircraft Systems Aviation Rulemaking Committee (Micro-ARC) ARC Recommendations Final Report dated 1 April 2016.

2. Details of Testing and Analysis Conducted to Develop Height-Velocity Limits

2.1. Overview of Approach for Developing Height-Velocity Limits

The Waiver Request shown in Appendix A of this report outlines the development of operating Height-Velocity limits for the Phantom 3 variants. These limits defined the safe operating envelope required to mitigate the risk of blunt trauma injuries following an aircraft failure when operating over people. This method includes initial ballistic analysis, estimation of drag coefficients for the ballistic models using CFD, refinement of the ballistic analysis based on CFD-generated flat plate drag areas, and ballistic model validation through flight test. The initial ballistic analysis was used to define test points to conduct UAS impact drop testing at the National Institute for Aviation Research (NIAR) at Wichita State University. The drop testing served to correlate injury potential for the recorded impact KE-levels with the abbreviated injury scale using automotive crash standards for injury. An extension of the NIAR drop testing is to determine energy absorption that could be used to correlate data with other KE standards such as the RCC. This section of the report does not intend to repeat all of the detailed data in the Waiver Request, but to highlight specifics of the tests not included in the request and summarize the results.

Additionally, the waiver request included design modifications implemented to limit the risk of laceration injuries due to blade strike. These were evaluated using a pendulum test to evaluate the limitations of these mitigations. The waiver request included analysis of critical contact points and operating considerations associated with the risk of penetration injuries following vehicle failure when operating over people. The details of the testing and analysis of these areas is included in this report along with a summary of the results.

2.2. Ballistic Modeling and CFD Analysis

Aerodynamic modeling and analysis of the vehicle was conducted to determine impact KE levels based on failure flight condition and vehicle attributes. The impact KE level is determined by the vehicle mass, flat plate drag areas (vertical and lateral). The second area of vehicle analysis is the estimated energy transfer to an impacted person. The energy transfer level is determined by the impact orientation, vehicle construction, and vehicle materials. The energy transfer levels are estimated based on conservation of momentum analysis of the vehicle's rebound trajectory and ATD Hybrid III dummy movement after impact. The CFD analysis is covered in the waiver request and will not be addressed in detail in this report. The CFD simulations reached converged solutions for all cases and yielded estimated drag coefficients for velocity sweeps in both orientations. The average coefficient of drag values for the Phantom 3 without guards is $C_{d,vert} = 0.9313$ and $C_{d,lat} = 1.077$. The average coefficient of drag values for the Phantom 3 with guards is $C_{d,vert} = 1.124$ and $C_{d,lat} = 1.122$. There is a 42% increase in the vertical flat plate drag area, and a 19.6% increase in the lateral flat plate drag area when the guards are added. This data

was used to update the aerodynamic model and create initial height-velocity diagrams based upon the results of flight testing.

2.3. Flight Testing

The purpose of performing flight tests was to collect data to validate the CFD and aerodynamic ballistic models. Two types of flight tests were performed, free fall from a hover and free fall following failure in translating flight, to characterize the ballistic trajectory of the aircraft in the event of an in-flight failure. Both types of tests required the aircraft to be unpowered, level in attitude, and at known initial velocities to capture accurate data. During the UAH flight testing, the aircraft was flown to the desired failure state and the operator performed a synchronized motor shut down. Three initial states were selected: 5 ft/s initial velocity, 10 ft/s initial velocity, and 20 ft/s initial velocity. All motor shut-offs were completed at approximately 400 ft AGL. Several iterations of each test profile were performed to account for winds and variability in the aircraft horizontal velocity at motor shutoff. The NIAR drop tests were used to validate ballistic model predictions for impact KE during a pure vertical descent.

These type of flight tests have a high risk of ground impact. For that reason, researchers modified a DJI Phantom 2 Standard airframe that had a damaged flight controller and GPS unit from previous flight tests instead of an off-the-shelf stock DJI Phantom 3 Advanced. The DJI Phantom 2 and 3 aircraft have the same external airframe shape and dimensions with the only differences being external payload options. A dummy camera was constructed from wood to replicate the mass and shape of the DJI Phantom 3 Advanced camera. A foam plug was constructed to replicate the mass and shape of the Vision Position System on the Phantom 3 Advanced.

The damaged Phantom 2 flight controller and GPS unit was removed and replaced with a 3D Robotics Pixhawk flight controller which also served the role as the onboard data logger. The stock Phantom 2 battery, motors, and electronic speed controllers (ESC) were re-used. A power distribution board was added to distribute the power from the Phantom main battery to each of the motors and the Pixhawk flight controller. The Pixhawk integration provided a simple solution for the synchronous motor shut down by relating a physical hardware switch on the pilot transmitter to a software command in the Pixhawk to instantly arm/disarm all motor outputs. This allowed for the aircraft to instantly return to a power setting proportional to the throttle stick position when re-armed from a motor-off free fall condition, bypassing the typical procedure of coordinated transmitter stick movements to arm/disarm the aircraft. This feature significantly reduced the pilot workload in recovering the aircraft from an unknown attitude. Alternatively, a radio controlled mechanical relay can be used on the ESC signal ground wire to disable the motors outputs for an aircraft that does not use the Pixhawk as a flight controller. A servo-release, spring launched parachute was installed on top of the aircraft to provide an alternate method of recovery in the event the aircraft could not be successfully re-armed from the free fall condition. A secondary battery was installed to keep the Pixhawk powered in the event of a

motor re-arm and parachute failure to prevent the loss of flight data if the main battery was ejected during a ground impact.

The 3DR Robotics Pixhawk flight controller is an open-source flight controller allowing custom vehicle integration, non-standard aircraft configurations, autonomous control, and full parameter data logging. Data from sensors on the Pixhawk main board is sampled and logged at 50 Hz, while the sample rate of external sensors is governed by the limitations of the sensor hardware. The externally connected 3DR GPS and magnetometer unit has a sample rate of 5 Hz. Pixhawk hardware configuration and flight data monitoring is managed through Mission Planner ground station software. Mission Planner has the ability to log flight data from the telemetry data received from the aircraft, however the sample rate is limited to the quality of the received telemetry data. Mission Planner also provides the utility to export log files for post processing. Optionally, individual flight data parameters can be reviewed and plotted within Mission Planner.

Flight tests were performed at locations that provide a controlled environment and airspace for operations, such as an AMA RC field or closed set flight area in Class G airspace. The minimum flight crew consisted of a pilot-in-command/pilot and a ground station operator (GSO). The role of the GSO is to provide the pilot with altitude and speed information during different segments of the flight and provide additional surveillance for hazards. The aircraft was flown manually in a stabilized, altitude-hold flight mode during all stages of the flight. Each test began at the maximum allowable altitude to increase the chances of a successful recovery.

For the static free fall tests conducted as part of the Task A4 effort, the GSO provided the pilot with altitude callouts until the target altitude was achieved. With the aircraft in a stable hover, the pilot toggled the transmitter switch to initiate the motor stop command. After allowing the aircraft to free fall without power for two seconds, the pilot toggled the transmitter switch to re-arm the motors. If the aircraft did not respond immediately and return to a stable attitude, the switch was toggled again to the disarm state at the same time the switch for the parachute deployment was activated. It was important to return the switch to a motor disarm state prior to deploying the parachute to prevent the parachute from becoming entangled in the propellers if the motors were to suddenly be re-armed.

For the tests simulating failure in translating flight, the GSO began reporting aircraft speed information upon the pilot's command after reaching the target altitude. The aircraft was slowly accelerated forward until the target initial velocity was achieved. The pilot would then toggle the switch to disarm the motors and allow the aircraft to fall for two seconds prior to beginning the recovery process.

Figure 1 shows good correlation between predicted falling flight trajectories from CFD developed flat plate drag area and the flight test data for the Phantom 3 with blade guards. Cross-winds during the test flight led to some discrepancies, but the comparison of a flight test

drop with an initial velocity of 27 ft/s corresponds well with the simulated drop with an initial velocity of 30 ft/s. The two drops with initial velocities of 6 ft/s and 7 ft/s are close to the simulation; however, the drop with light green markers appears to have experienced gusts during the drop. Overall, the ballistic model, driven by CFD flow field simulation, produces accurate data outputs that are validated by both vertical drops and forward flight failure test flights.

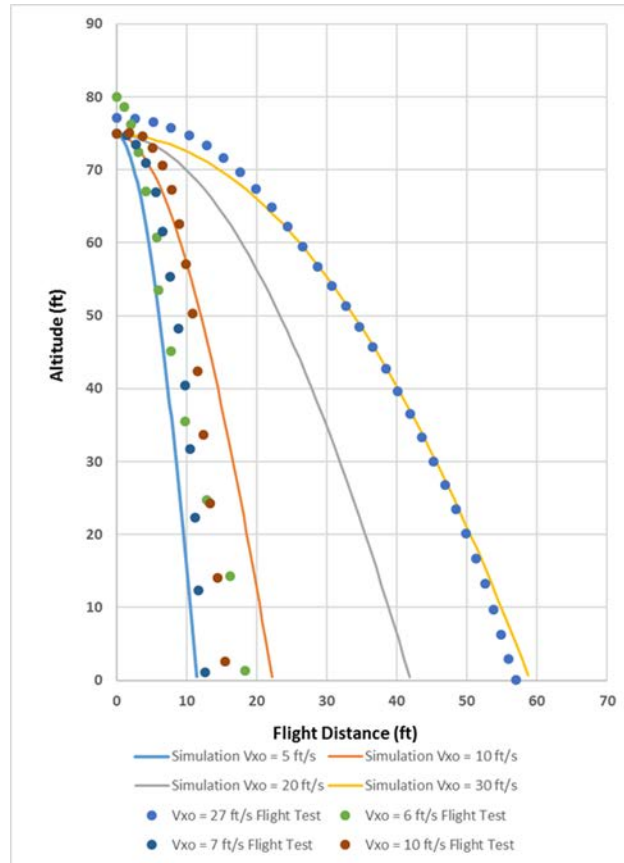


Figure 1- Comparison of Simulation and Flight Test Results

2.4. NIAR Drop Testing

2.4.1. Test Setup

Wichita State University’s (WSU) National Institute for Aviation Research (NIAR) conducted a series of vehicle drop tests on the head of an ATD Hybrid III 50th Percentile Male Crash Test Dummy.³ The testing consisted of 24 complete tests using a DJI Phantom 3 Standard striking the test dummy to simulate a vehicle collision with a person based on a range of failure flight conditions. NIAR conducted two tests that were considered no tests, for a 30-foot vertical drop

³ Humanetics Innovative Solutions. (08/30/2016) *Hybrid III 50th Male Dummy*. Retrieved from <http://www.humaneticsatd.com/crash-test-dummies/frontal-impact/hybrid-iii-50th>.

and a 62° impact angle drop. These two tests yielded dummy instrument readings, but did not produce any high-speed video or photometric data and as such were deemed as no tests. Table 1 summarizes all of the completed testing. The dummy's instrumentation and data outputs, along with additional collision sequence photometric data are summarized in Appendix A – UAH Part 107 Waiver Submission for Flight Over People. In addition to the photometric data of the UAS collision sequences and test reports that include dummy head and neck impact loading, force vs. time, and angular rate vs. time data, NIAR provided high speed videos of each collision.

Figure 2 shows a diagram of the drop test equipment setup at NIAR. The sled is a large metal slab that serves as the mounting point for the drop rail uprights, seat and dummy (the dummy is annotated as “ATD” in the diagram). The cameras provided the photometric tracking data to give instantaneous translational and angular velocities of the UAS for a short duration before and after each impact. Figure 3 shows the basic setup from the front right. This figure also shows the impact orientation of the Phantom 3 with respect to the dummy's head for the vertical, horizontal, and angled impact testing. The UAS impacted directly on top of the head with the payload during all vertical drop testing. The vertical drop testing replicated a UAS failure in hover with the aircraft falling in a level attitude. The angled drop testing replicated a UAS failure in forward flight. For the angle impact tests, the dummy seat was tilted back by either 58° or 62°. The UAS was dropped vertically with an attitude of 58° or 62°. In this way, it replicated an impact with level attitude while descending with the desired impact trajectory angle. This type of impact is characteristic of the Phantom 3, which tends to fall with a level attitude after a complete loss of power.⁴ During the horizontal impact tests, the UAS struck the dummy on the forehead, with area between the vehicle arms as the point of contact. A pendulum was used to accelerate the UAS to impact speed prior to horizontal impact with the dummy's head. The UAS was resting on low friction rails so that it would continue moving toward the dummy's head after the pendulum swing was arrested in the horizontal impact tests.

⁴ FAA A4 Project Team, White Paper on UAS Characteristics for the FAA UAS Center of Excellence Task A4: Ground Collision Severity Evaluation, June 3, 2016

Table 1 - UAS Drop Testing Summary

Test Details				
NIAR Test Number	Test Number	Orientation	Height	Velocity
UA17A-01	V(90)-20-1	Vertical	20 ft	
UA17A-02	V(90)-20-2	Vertical	20 ft	
UA17A-03	V(90)-20-3	Vertical	20 ft	
UA17A-04	NO TEST	Vertical	30 ft	
UA17A-05	V(90)-30-1	Vertical	30 ft	
UA17A-06	V(90)-30-2	Vertical	30 ft	
UA17A-07	V(90)-30-3	Vertical	30 ft	
UA17A-08	V(90)-40-1	Vertical	40 ft	
UA17A-09	V(90)-40-2	Vertical	40 ft	
UA17A-10	V(90)-40-3	Vertical	40 ft	
UA17A-11	V(90)-50-1	Vertical	50 ft	
UA17A-12	V(90)-50-2	Vertical	50 ft	
UA17A-13	V(90)-50-3	Vertical	50 ft	
UA17A-14	H(0)-4.5-1	Horizontal		17 ft/s
UA17A-15	H(0)-4.5-2	Horizontal		17 ft/s
UA17A-16	H(0)-4.5-3	Horizontal		17 ft/s
UA17A-17	A(65)-36.5-1	62 deg		36.5 ft/s
UA17A-18	A(65)-36.5-2	62 deg		36.5 ft/s
UA17A-19	NO TEST	62 deg		36.5 ft/s
UA17A-20	A(65)-36.5-4	62 deg		36.5 ft/s
UA17A-21	A(58)-46.1-1	58 deg		46.1 ft/s
UA17A-22	A(58)-46.1-2	58 deg		46.1 ft/s
UA17A-23	A(58)-46.1-3	58 deg		46.1 ft/s
UA17A-24	A(58)-51.7-1	58 deg		51.7 ft/s
UA17A-25	A(58)-51.7-2	58 deg		51.7 ft/s
UA17A-26	A(58)-51.7-3	58 deg		51.7 ft/s

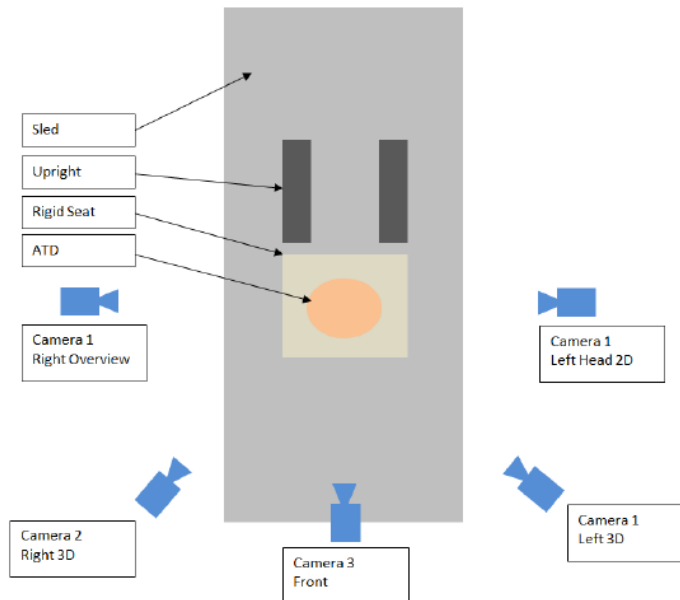


Figure 2 - Top View of Sled Setup for UAS Drop



Figure 3 - Front Left View of Sled Setup (upper left), Vertical Drop Position of Dummy and UAS (upper right), Pendulum Setup for Horizontal Impact Test (lower left), and Dummy and UAS Setup for Angle Impact Test (lower right)

2.4.2. NIAR Report Content

NIAR provided comprehensive reports on all 26 tests of which two tests were considered no tests. NIAR summarized all test findings into a 480 page, final report⁵ that is not included in this document, but will be submitted to the FAA at the time this report is submitted. Instrumentation and data collected during each test is shown in Table 2 below. Analysis of the data for each test report is provided as a summary table and time histories as shown in Figure 4 and Figure 5, respectively.

⁵ Huculak, R., NIAR UAS Drop Testing Report, Doc. CDL-TR-17-2163-UA01, 19 August 2016.

Table 2 - NIAR Instrumentation for UAS Drop Tests

Instrumentation		
Type	Location	Direction
Accelerometer	Head	Ax
		Ay
		Az
Angular Rate Sensor	Head	Rx
		Ry
		Rz
Load Cell	Upper Neck	Fx
		Fy
		Fz
		Mx
		Mz
Velocity Gate	UAS	Resultant

Photometric Analysis

Location	Orientation
ATD Head	2D - XZ
UAS	3D

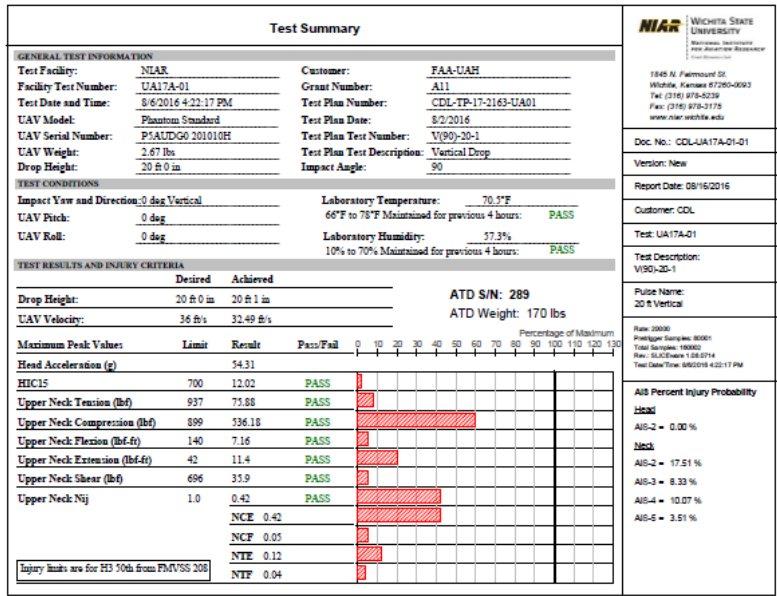


Figure 4 - Example NIAR Test Summary for an Individual Test

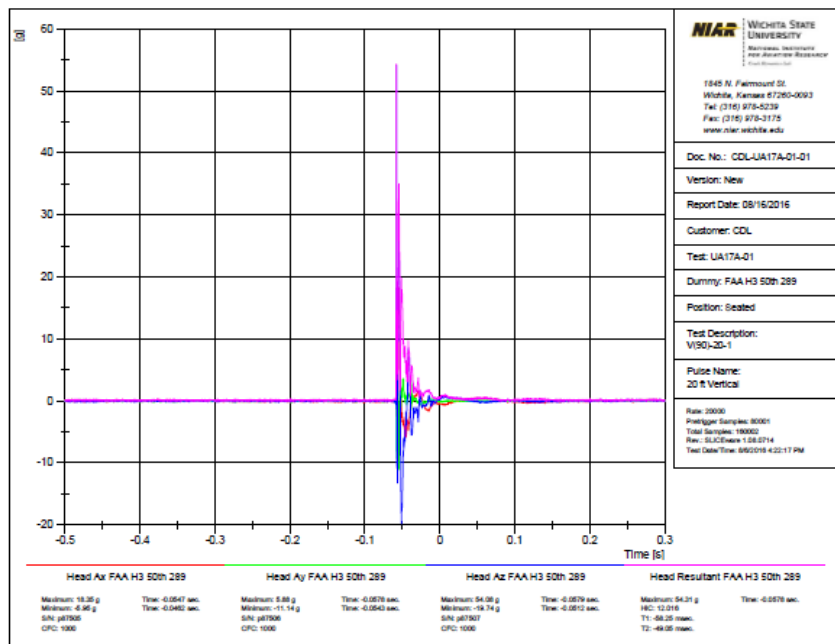


Figure 5 - Example NIAR Time History for an Individual Test

2.4.3. Correlation of Impact Loads and Accelerations with Injury Metrics

The injury potential for specific impact KEs and impact angles was evaluated using injury metrics established by the National Highway Traffic Safety Administration (NHTSA), National Transportation Biomechanics Research Center (NTBRC) in November 1999.⁶ The NHTSA study was conducted to upgrade the Federal Motor Vehicle Safety Standard (FMVSS) No. 208⁷ frontal crash protection safety standard. “Based on the agency’s analysis of comments received in response to the publication of the NPRM and the accompanying technical reports, the agency has made modifications to the recommended injury criteria and their associated performance limits.... This report, which is a supplement to the previous report, “Development of Improved Injury Criteria for the Assessment of Advanced Automotive Restraint Systems”, (Kleinberger, et al, NHTSA Docket 98-4405-9) documents these modifications and the rationale.”⁶

The NHTSA report utilizes the Abbreviated Injury Scale (AIS)⁸ called out in the Micro-ARC Final Report¹ to establish the injury potential of forces caused by the impact KE of the UAS striking the 50th percentile ATD crash dummy³ placed in the seated position. While automotive crashes are systematically different in their causation, the impact forces to the crash dummy have formed the basis for these injury assessments, versus the causation that created the forces. The

⁶ Eppinger, R., Sun, E., Bandak, F., Haffner, M., Khaewpong, N., Maltese, M., Kuppa, S., Nguyen, T., Takhounts, E., Tannous, R., Zhang, A., Saul, R., Development of Improved Injury Criteria for the Assessment of Advanced Automotive Restraint Systems – II, November 1999.

⁷ <http://www.nhtsa.gov/cars/rules/import/FMVSS/#SN208>

⁸ Association for the Advancement of Automotive Medicine Website, <http://www.aaam.org/about-ais.html>

automotive standards were utilized because of their well-established injury metrics correlated with the AIS since UAS injuries have no substantial database for tracking such injury potential based upon the forces applied to the body. Furthermore, the Micro-ARC Category 3 and Category 4 Performance Standards¹ recommended an injury metric that included no greater than a 30% chance of AIS Level 3 injury or greater following impact with a non-participant. The drop tests and the use of the automotive injury metrics provided the first basis for correlating UAS impact KE with the AIS to address these performance standards.

Table 3 - NIAR Summary Test Results and Injury Metrics

Test Number	UAV Weight (lbs)	Impact Velocity (fps)	Impact KE (ft-lbs)	Impact Angle (deg)	Maximum Resultant Head Acceleration (g)	HIC15 (Max 700)	Probability of Head Injury P(AIS≥2)	Probability of Neck Injury P(AIS≥2)	Probability of Neck Injury P(AIS≥3)	Probability of Neck Injury P(AIS≥4)	Probability of Neck Injury P(AIS≥5)
UA17A-01 V(90)-20-1	2.69	32.49	44.1	90	54.31	12.02	0.00%	17.48%	8.32%	10.05%	3.50%
UA17A-02 V(90)-20-2	2.69	32.31	43.6	90	56.68	14.99	0.00%	18.00%	8.78%	10.38%	3.63%
UA17A-03 V(90)-20-3	2.69	32.5	44.2	90	49.18	15.64	0.00%	18.36%	9.10%	10.60%	3.71%
UA17A-05 V(90)-30-1	2.69	39.25	64.4	90	47.78	19.29	0.00%	18.54%	9.26%	10.72%	3.76%
UA17A-06 V(90)-30-2	2.69	39	63.6	90	48.35	23.45	0.00%	20.02%	10.68%	11.67%	4.12%
UA17A-07 V(90)-30-3	2.69	38.74	62.7	90	66.36	23.02	0.00%	18.18%	8.94%	10.49%	3.67%
UA17A-08 V(90)-40-1	2.69	43.08	77.6	90	78.7	46.62	0.01%	21.40%	12.06%	12.56%	4.46%
UA17A-09 V(90)-40-2	2.69	43.21	78.1	90	54.01	34.13	0.00%	21.80%	12.49%	12.82%	4.56%
UA17A-10 V(90)-40-3	2.69	43.96	80.8	90	78.62	42.79	0.01%	20.22%	10.86%	11.79%	4.16%
UA17A-11 V(90)-50-1	2.69	49.58	102.8	90	82.38	59.54	0.03%	21.80%	12.49%	12.82%	4.56%
UA17A-12 V(90)-50-2	2.69	49.17	101.1	90	71.5	48.04	0.01%	21.20%	11.86%	12.43%	4.41%
UA17A-13 V(90)-50-3	2.69	49.14	100.9	90	119.13	42.24	0.01%	21.40%	12.06%	12.56%	4.46%
UA17A-14 H(0)-4.5-1	2.69	17.25	12.4	0	25.05	7.83	0.00%	12.36%	4.44%	6.93%	2.36%
UA17A-15 H(0)-4.5-2	2.69	17.25	12.4	0	60.65	29.18	0.00%	12.63%	4.61%	7.08%	2.42%
UA17A-16 H(0)-4.5-3	2.69	17.2	12.4	0	43.18	19.94	0.00%	12.49%	4.52%	7.01%	2.39%
UA17A-17 A(65)-36.5-1	2.69	37.03	57.3	65	60.12	39.55	0.01%	19.46%	10.12%	11.30%	3.98%
UA17A-18 A(65)-36.5-2	2.69	36.8	56.6	65	60.88	0.04	0.00%	19.27%	9.95%	11.18%	3.93%
UA17A-20 A(65)-36.5-4	2.69	36.56	55.9	65	55.64	26.25	0.00%	19.08%	9.77%	11.07%	3.89%
UA17A-21 A(58)-46.1-1	2.69	45.95	88.3	58	112.69	107.94	0.35%	19.46%	10.12%	11.30%	3.98%
UA17A-22 A(58)-46.1-2	2.69	46.06	88.7	58	120.49	119.07	0.49%	18.90%	9.60%	10.95%	3.84%
UA17A-23 A(58)-46.1-3	2.69	46.06	88.7	58	130.47	147.82	1.01%	19.27%	9.95%	11.18%	3.93%
UA17A-24 A(58)-51.7-1	2.69	50.37	106.1	58	119.79	137.17	0.79%	18.54%	9.26%	10.72%	3.76%
UA17A-25 A(58)-51.7-1	2.69	50.48	106.5	58	139.15	165.07	1.41%	18.90%	9.60%	10.95%	3.84%
UA17A-26 A(58)-51.7-1	2.69	50.46	106.4	58	126.58	123.64	0.56%	18.90%	9.60%	10.95%	3.84%

Note: Colors in the table represent the magnitude of the individual entry with green being the lowest values and red being the highest values within a column.

A summary of the NIAR test results and injury metrics are shown in Table 3. The observed impact KE values in the NIAR testing correlate to no greater than 12.5% probability of an AIS Level 3 injury or greater based on the NHTSA standards. The probability of skull fracture, based

on these impact KE-levels, was substantially lower at a probability less than 1.5%. The injury metrics from the NIAR tests for both skull fracture and neck injuries provide substantial margin to the Micro-ARC injury thresholds established for Category 3 and 4 operations with the most likely injury potential being AIS Level 2 or less injury.

The results of the tests showed significant discrepancy with the levels of safety assessed utilizing the impact KE values extracted from the PoF charts in RCC 321-00¹⁰ shown in Figure 6, the levels of safety derived using the RCC Area Weighted Approach shown in Figure 7 and Figure 8, and those derived using a modified Area Weighted impact KE Approach in the UAS Characteristics White Paper.⁴ The discrepancies are shown in Table 4.

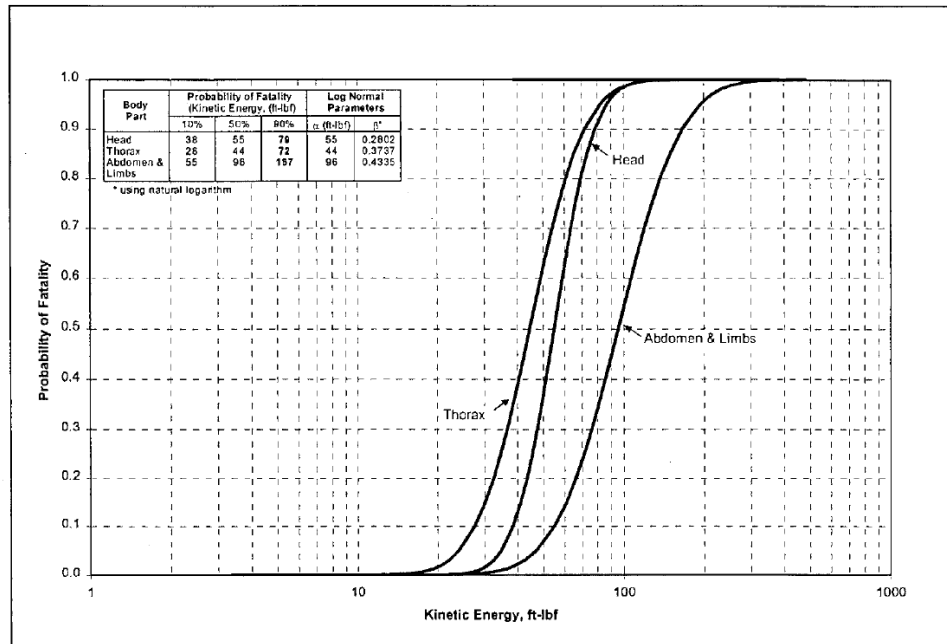


Figure 6 - Probability of Fatality from Debris Impacts for Various Body Parts from RCC 321-00⁹

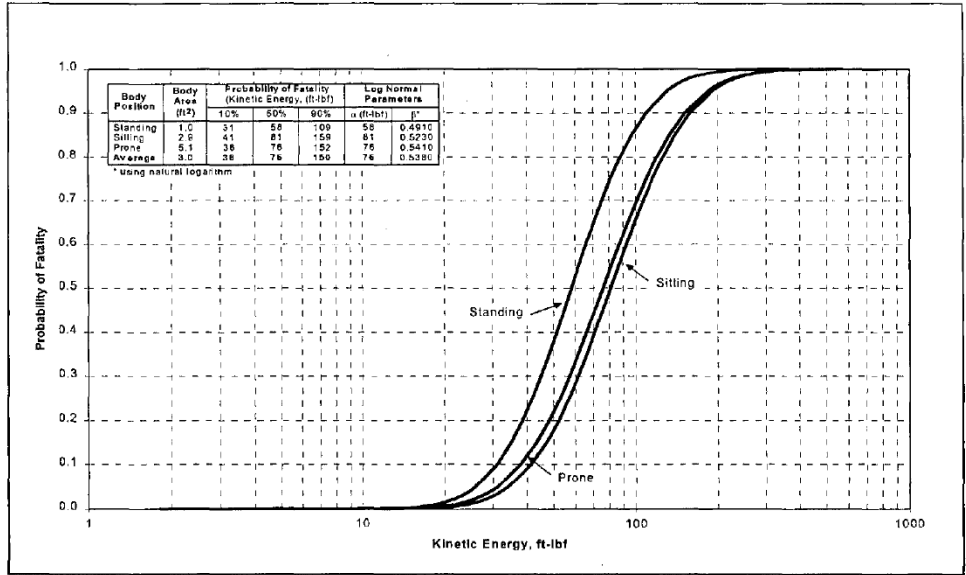


Figure 7 - Probability of Fatality from Debris Impacts for Various Body Positions⁹

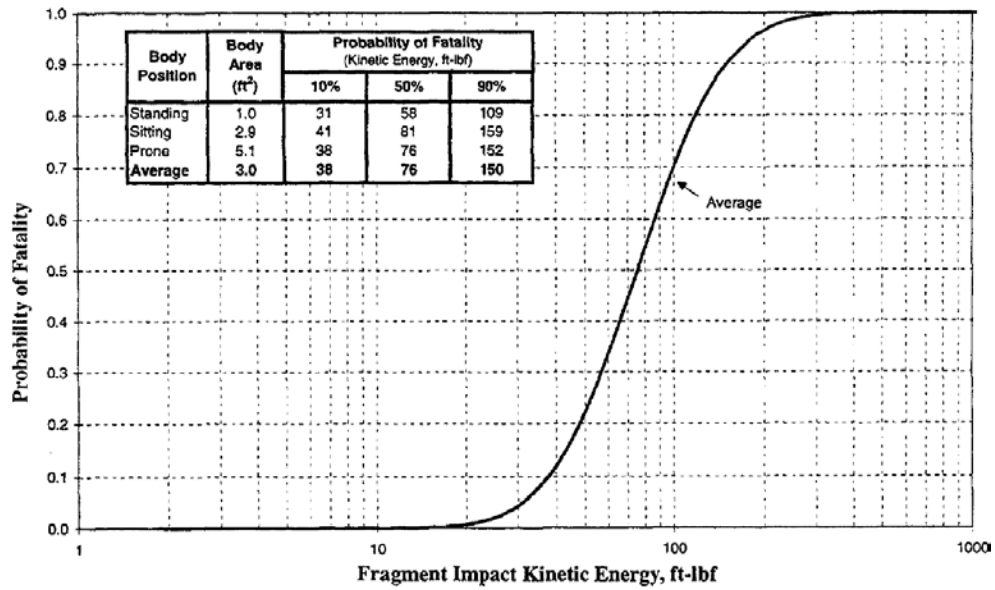


Figure 8 - Average Probability of Fatality from Debris Impacts

Table 4 - Difference in Injury Metrics Between FMVSS 208 and RCC Standards

Test Number	UAV Weight (lbs)	Impact Velocity (fps)	Impact KE (ft-lbs)	FMVSS 208 Standards				RCC Standards for PoF			Area Weighted PoF		
				Probability of Neck Injury P(AIS≥2)	Probability of Neck Injury P(AIS≥3)	Probability of Neck Injury P(AIS≥4)	Probability of Neck Injury P(AIS≥5)	Head	Thorax	Body and Limbs	Standing	Sitting	Rock Concert
UA17A-01 V(90)-20-1	2.69	32.49	44.1	17.48%	8.32%	10.05%	3.50%	21.5%	50.2%	3.6%	6.2%	9.6%	19.5%
UA17A-02 V(90)-20-2	2.69	32.31	43.6	18.00%	8.78%	10.38%	3.63%	20.4%	49.0%	3.4%	5.8%	9.1%	18.7%
UA17A-03 V(90)-20-3	2.69	32.5	44.2	18.36%	9.10%	10.60%	3.71%	21.8%	50.5%	3.7%	6.2%	9.6%	19.6%
UA17A-05 V(90)-30-1	2.69	39.25	64.4	18.54%	9.26%	10.72%	3.76%	71.3%	84.6%	17.9%	26.3%	36.0%	56.9%
UA17A-06 V(90)-30-2	2.69	39	63.6	20.02%	10.68%	11.67%	4.12%	69.8%	83.8%	17.1%	25.3%	34.8%	55.5%
UA17A-07 V(90)-30-3	2.69	38.74	62.7	18.18%	8.94%	10.49%	3.67%	68.0%	82.8%	16.3%	24.3%	33.6%	54.0%
UA17A-08 V(90)-40-1	2.69	43.08	77.6	21.40%	12.06%	12.56%	4.46%	89.0%	93.6%	31.2%	42.6%	54.2%	75.1%
UA17A-09 V(90)-40-2	2.69	43.21	78.1	21.80%	12.49%	12.82%	4.56%	89.5%	93.8%	31.7%	43.2%	54.8%	75.6%
UA17A-10 V(90)-40-3	2.69	43.96	80.8	20.22%	10.86%	11.79%	4.16%	91.5%	94.8%	34.5%	46.4%	58.2%	78.4%
UA17A-11 V(90)-50-1	2.69	49.58	102.8	21.80%	12.49%	12.82%	4.56%	98.7%	98.8%	56.3%	68.6%	78.9%	92.4%
UA17A-12 V(90)-50-2	2.69	49.17	101.1	21.20%	11.86%	12.43%	4.41%	98.5%	98.7%	54.8%	67.2%	77.7%	91.7%
UA17A-13 V(90)-50-3	2.69	49.14	100.9	21.40%	12.06%	12.56%	4.46%	98.5%	98.7%	54.6%	67.1%	77.7%	91.7%
UA17A-14 H(0)-4.5-1	2.69	17.25	12.4	12.36%	4.44%	6.93%	2.36%	0.0%	0.0%	0.0%	<1%	<1%	<1%
UA17A-15 H(0)-4.5-2	2.69	17.25	12.4	12.63%	4.61%	7.08%	2.42%	0.0%	0.0%	0.0%	<1%	<1%	<1%
UA17A-16 H(0)-4.5-3	2.69	17.2	12.4	12.49%	4.52%	7.01%	2.39%	0.0%	0.0%	0.0%	<1%	<1%	<1%
UA17A-17 A(65)-36.5-1	2.69	37.03	57.3	19.46%	10.12%	11.30%	3.98%	55.8%	76.0%	11.7%	18.0%	25.8%	44.3%
UA17A-18 A(65)-36.5-2	2.69	36.8	56.6	19.27%	9.95%	11.18%	3.93%	54.1%	75.0%	11.1%	17.2%	24.8%	42.9%
UA17A-20 A(65)-36.5-4	2.69	36.56	55.9	19.08%	9.77%	11.07%	3.89%	52.3%	73.9%	0.0%	16.5%	23.8%	41.5%
UA17A-21 A(58)-46.1-1	2.69	45.95	88.3	19.46%	10.12%	11.30%	3.98%	95.4%	96.9%	42.4%	54.8%	66.6%	84.7%
UA17A-22 A(58)-46.1-2	2.69	46.06	88.7	18.90%	9.60%	10.95%	3.84%	95.6%	97.0%	42.8%	55.3%	67.0%	85.0%
UA17A-23 A(58)-46.1-3	2.69	46.06	88.7	19.27%	9.95%	11.18%	3.93%	95.6%	97.0%	42.8%	55.3%	67.0%	85.0%
UA17A-24 A(58)-51.7-1	2.69	50.37	106.1	18.54%	9.26%	10.72%	3.76%	99.0%	99.1%	59.1%	71.3%	81.1%	93.5%
UA17A-25 A(58)-51.7-1	2.69	50.48	106.5	18.90%	9.60%	10.95%	3.84%	99.1%	99.1%	59.5%	71.6%	81.4%	93.7%
UA17A-26 A(58)-51.7-1	2.69	50.46	106.4	18.90%	9.60%	10.95%	3.84%	99.1%	99.1%	59.4%	71.6%	81.4%	93.6%

Notes:

- 1) Color coding of Impact KE is based upon magnitude of KE in comparison to the data listed with the lowest being green and the highest being red.
- 2) Color coding of injury metrics is as follows: Green (0-30%), Yellow (30-50%) and Red (Greater than 50%)

It is important to recognize that the FMVSS 208 standards were developed to analyze impacts to the ATD crash dummies for the range of vehicle crash tests (minor to severe). The ATD data collected during crash testing is correlated with injury data contained in the AIS database as reported by medical professionals who have experience with injury severity and, most importantly, the mortality resulting from such injuries. While automotive crashes are not the same as those of the a UAS ground collision, the impact forces and physics as it relates to the ATD crash dummy are the same and, justifiably, can be analytically evaluated against similar injury metrics associated with automobile accidents until sufficient UAS data becomes available. Consider that the RCC^{9,10} PoF metrics established for various impact KE were established from debris analysis with little or no correlation to significant databases associated with injury metrics similar to AIS. To clarify the basis for the establishment of the RCC standards in comparison to the FMVSS 208 standards, it is important to understand how the RCC Standards were developed.

2.4.4. Evolution of RCC Standards and Their Applicability to UAS Ground Collisions.

Most other KE values found in the literature trace back to one of two studies – either Feinstein¹¹ or Janser¹². Both of these studies developed a quantitative assessment of PoF of injuries based on fragment velocity and mass associated with debris studies from explosions to assist in safety assessments. These studies compare the various probabilities of fatality based on the body region (head, thorax, abdomen, or limbs) that is impacted by the debris. While it is not explicitly stated, the more conservative numbers from Feinstein’s work¹¹ may be why they were selected for use in RCC standards. Of note, the Feinstein values¹¹ were the basis for developing the 10%, 50%, and 90% PoF values in RCC documents. Feinstein’s data was developed by analyzing data produced by other researchers who conducted projectile impact testing on live animals and animal carcasses, whereas the source of Janser’s data is not laid out as clearly. It is much harder to qualify the accuracy of Janser’s content¹² because of this fact.

RCC 321-00^{9,10} published common risk standards for the National Test Ranges and utilized the PoF for various impact KEs as shown in Figure 6. These curves were combined with an area weighting from the Janser Standard Man¹² to develop a S-curve for each body position since each body part alone does not have an equal probability of being hit by debris based upon a person’s position; sitting, standing and prone, as shown in Figure 7. The weighted approach allows for a better assessment of fatalities by accounting for the probability of the debris hitting different body areas as well as accounting for different impact angles that can be assessed through the impact KE values shown in Figure 7.⁹ The RCC further modified the curve by

⁹ Range Commander’s Council, Supplement to Standard 321-00 “Common Risk Criteria for National Test Ranges; Inert Debris”, April 2000

¹⁰ Range Commander’s Council, Standard 321-00 “Common Risk Criteria for National Test Ranges; Inert Debris”, April 2000

¹¹ Feinstein, D. L., Heugel, W.F., Kardatzke, M.L. Weinstock, A. Personnel Casualty Study, IITRI Project No. J6067 Final Report

¹² Janser, P.W. Lethality of Unprotected Persons Due to Debris and Fragments, Twentieth Explosives Safety Seminar, August 1982

averaging the probability for each body position into a composite curve as shown in Figure 8. Figure 8 was specifically developed by the RCC because of the uncertainty associated with which body positions might be encountered in any given impact scenario. Figure 8 represents an equal weighting of the standing, sitting and prone positions based upon Figure 7 and was deemed by Sandia and the RCC to represent conservative values for PoF since most situations involving collision in populated areas has a mixed distribution of people in different orientations and standing and sitting can also represent differences in impact angles.¹³ The development of these curves from Feinsein's original work was conducted by Sandia Labs¹³ and these curves remain part of the RCC standards today. The limitations of the RCC standards are rooted in the fundamental assumptions made to generate the curves and the basis for PoF data.

Sandia Labs was part of the Risk and Lethality Commonality Team (RALCT) that was formed in 1996 to address safety concerns related to the generation of inert debris by flight tests at national ranges.¹³ The debris analysis required by the national test ranges, "...can vary from hardware shed during normal missile operation to fragments generated by explosion, hypervelocity collision, aerothermal breakup, or a flight termination system."¹³ The RCC plots were developed from Feinsein's data and employed weightings for hypervelocity type collisions where the debris contained a larger number of low mass fragments. Figure 6, Figure 7, and Figure 8 represent the weighted KE values for these more numerous, smaller mass fragments. Furthermore, the analysis conducted by the RCC and Sandia Labs shows that the inert debris impacts were largely vertical since it was assumed that the breakup or collisions would occur at very high altitudes. Sandia Labs recommended that the data set and analysis which culminated in Figure 6, Figure 7, and Figure 8 be utilized by range safety personnel until more accurate data and predictive tools for evaluating large mass (> 2lbs) impact on people is developed.¹³ The testing and analysis of the UAS impacts with the ATD dummy against the FMVSS standards forms the initial basis for a better approach to understanding injuries associated with UAS impacts then utilizing fragment analysis from in-flight breakup of hypervelocity missiles.

2.4.5. Differences Between UAS Collisions and Low Mass, High Volume Debris Following In-flight Breakup

Small UAS (sUAS) ground collisions do not occur due to an inflight breakup at high altitudes with a large quantity of small mass fragments, but rather sUAS platforms tend to have collisions at lower speeds where the whole platform strikes an individual somewhere on the exposed portions of the individual's body. Two fundamental UAS characteristics are addressed to show how the RCC PoF metrics may be excessively conservative, as shown by the NIAR results; 1) a sUAS has larger contact area than that of small debris fragments resulting in less severe injuries for a given impact KE and 2) crash geometries and the elasticity of sUAS cause collisions to be dramatically different than solid, small mass fragments. Crash geometries are defined as the

¹³ Cole, J.K., L.W. Young, and T. Jordan-Culler. "Hazards of Falling Debris to People, Aircraft, and Watercraft." Sandia National Laboratory. 1997. doi:10.2172/468556.

orientation, impact angle and multiple contact areas that define how energy is transferred to the individual during the collision

2.4.5.1. Larger Contact Area of UAS vs. Fragments.

The physiological data upon which Feinstein based his analyses were obtained from experiments that had been performed for the Department of Defense on live animals, human cadavers, and skin and gelatin models to determine the injury potential of various blast fragments associated with explosions or blast effects due to an explosion or nuclear blast wave. Tests with animals, human cadavers/skulls were conducted using small ball type projectiles, glass fragments shot from Styrofoam sabots¹⁴ and dropping subjects/test articles from various heights to create sufficient impact energy necessary for the test. The effect of the larger contact area of the sUAS, when compared to small mass projectiles and glass fragments, is illustrated by way of data published by Fugelso.¹⁵ The data in Table 5 compares various projectiles falling at terminal velocity or propelled to higher velocities are based on their ability to penetrate skin and cause blunt trauma resulting in liver fractures. The baseball and golf ball have substantially higher KE when falling at terminal velocity; however, the larger contact area and curved surfaces have extremely low probability of penetrating bare skin and no likelihood of liver fractures when compared with smaller particles such as a penny and nut & bolt that have much lower KE values at terminal velocities, but have a 100% chance of penetrating bare skin and some chance of causing liver fractures. Furthermore, the larger contact areas of small mass fragments versus a full size sUAS prevents the vehicle from striking specific body parts, which is especially true when impact angles are steep. The sUAS physical geometry results in numerous contact points during a collision when descending at impact angles above horizontal, making impacts on single body parts such as the thorax implausible. For example, the use of blade guards on arms extending away from the main body of the sUAS and landing gear extending down from the sUAS creates barriers to striking small contact areas such as the throat area such that bilateral hemorrhage of carotid arteries is highly unlikely to occur. Bilateral hemorrhage of the thorax was one of the injuries used in the creation of the Feinstein data for the thorax.¹¹ Injuries to the thorax become increasingly less plausible when the sUAS is descending at angles greater than 45 degrees. For the waiver submitted for the Phantom 3 Standard and Advanced, the descent angles were greater than 58 degrees, which further reduces the likelihood of any significant impact to the thorax when compared to small fragment projectiles moving horizontally at similar kinetic energies. The use of the thorax impact KE as the sole means of defining regulatory thresholds is excessively conservative in the context of credible impact scenarios and their resulting injury potential for blunt force trauma. The regulatory framework should consider that

¹⁴ White, C. S., Bowen, G. I. and Richmond, D. R., Biological Tolerance to Air Blast and Related Biomedical Criteria, Lovelace Foundation, April 1965, U. S. Atomic Energy Commission CEX-65.4.

¹⁵ Fugelso, L. M., Weiner, L. M., and Schiffman, T. H., *Explosive Effects Computation Aids*, Final Report GARD Project No. 1540, General American Research Division, General American Transportation Corp, Niles, IL.

the potential of laceration injuries to the thorax has a greater likelihood of creating bilateral hemorrhage than blunt force trauma injuries caused by impact KE. The waiver process standards included in this document address appropriate methods for mitigating laceration injuries.

Comparing injury potential of sUAS to data developed from blast fragments with penetration potential and small contact areas does not result in similar contact or collision scenarios that are appropriate for evaluating sUAS. The NIAR tests are actual sUAS collisions that provide actual impact data which is correlated to automotive injury data similar in injury type and forces on the ATD dummy that are more similar to sUAS impacts with a human.

Table 5 - Injury Characteristics for Some Common Objects¹³

	Object Impacting	Mass (gm)	Velocity (fps)	Area (in ²)	Kinetic Energy (ft-lbf)	Probability of Bare Skin Penetration	Likelihood of Liver Fracture ⁺
Terminal Velocity	Warhead Canister	2600	279	9.0	6936	1.000	Large
	Cable (6ft x 1 in)	1590	77	71.3	323	0.002	Some
	38 Cal. Bullet	16	432	0.11	102	1.000	Large
	30 Cal. Bullet	12	473	0.07	92	1.000	Large
	Warhead Fragment	70	174	0.62	73	0.966	Some
	Baseball	145	109	6.5	59	0.015	No
	Golf Ball	46	106	2.2	18	0.011	No
	22 Cal. Bullet	3	329	0.037	11	1.000	Some
	Penny	3	309	0.42	9.8	1.000	Some
	Nut & Bolt	14	93	0.44	4.1	0.018	No
Propelled	22 Cal. Bullet	3	1476	0.037	224	1.000	Large
	Golf Ball	46	249	2.2	98	0.632	Some
	90 mph Fast Ball	145	132	6.5	87	0.045	Some

* Probability of bare skin penetration and liver fracture based on data of Neades and Rudolph.²⁸

+ Assuming a body mass around 68 kg (150 lbs).

2.4.5.2. Crash Geometries and the Elasticity of UAS

sUAS platforms are predominantly made of various forms of plastic and foam materials as characterized by the various categories of UAS described in the A4 UAS Characteristics White Paper.⁴ Multi-rotor sUAS are dominated by this type of design and are characterized by significant flexibility in their structures and fragility of their payloads during ground collisions. Many fixed wing platforms are made of foam material and break-away wings that further reduce impact forces over those characterized by solid, metal debris fragment masses used to develop the PoF metrics in the RCC standards. sUAS fuselages are not fabricated from large amounts tungsten, aluminum or steel as might be observed from an in-flight breakup of a

missile on one of the national test ranges. While the motors of sUAS are made of these types of materials, the motors are rarely the surface or material that is in contact with a human during a ground collision event. Furthermore, the motors are attached to flexible structures especially in monocoque fuselage multi-rotor UAS, like the Phantom 3, resulting in less impact energy if they do contact the human as part of the impact event. A review of the resultant loads from the NIAR tests can also be used to show how these characteristics of a sUAS are substantially different than those of low mass, metallic fragment impact as they relate to skull fracture. Table 6 and Figure 9 shows the resultant head loads as calculated for the 10 lbs head of the ATD Hybrid III 50th Percentile test dummy.

Table 6 - Resultant Head Forces from NIAR Tests

Test Number	UAV Weight (lbs)	Impact Velocity (fps)	Impact KE (ft-lbf)	Impact KE (N-m)	Impact Angle (deg)	Maximum Resultant Head Acceleration (g)	Maximum Resultant Head Force (lbf)	Maximum Resultant Head Force (N)	Sample Mean KE (ft-lbf) μ	Sample Standard Deviation KE (ft-lbf) σ	Sample Mean Resultant Load Factor (g) μ	Sample Standard Deviation of Resultant Load Factor (g) σ	Max Load Factor (g)	Calculated Maximum Induced Load Factor (g)	3 σ Resultant Load Factor (g)
UA17A-01 V(90)-20-1	2.67	32.49	43.8	59.4	90	54.31	727.754	3237.2	43.6	0.29	53.4	3.8	56.7	49.5	64.9
UA17A-02 V(90)-20-2	2.67	32.31	43.3	58.7	90	56.68	759.512	3378.5							
UA17A-03 V(90)-20-3	2.67	32.5	43.8	59.4	90	49.18	659.012	2931.4							
UA17A-05 V(90)-30-1	2.67	39.25	63.9	86.7	90	47.78	640.252	2848.0	63.1	0.83	54.2	10.6	66.4	71.6	85.9
UA17A-06 V(90)-30-2	2.67	39	63.1	85.6	90	48.35	647.89	2882.0							
UA17A-07 V(90)-30-3	2.67	38.74	62.3	84.4	90	66.36	889.224	3955.5							
UA17A-08 V(90)-40-1	2.67	43.08	77.0	104.4	90	78.7	1054.58	4691.0	78.2	1.72	70.4	14.2	78.7	88.7	113.1
UA17A-09 V(90)-40-2	2.67	43.21	77.5	105.0	90	54.01	723.734	3219.3							
UA17A-10 V(90)-40-3	2.67	43.96	80.2	108.7	90	78.62	1053.508	4686.2							
UA17A-11 V(90)-50-1	2.67	49.58	102.0	138.3	90	82.38	823.8	3664.4	100.8	1.01	91.0	25.0	119.1	114.4	165.9
UA17A-12 V(90)-50-2	2.67	49.17	100.3	136.0	90	71.5	958.1	4261.8							
UA17A-13 V(90)-50-3	2.67	49.14	100.2	135.8	90	119.13	1596.342	7100.9							
UA17A-14 H(0)-4.5-1	2.67	17.25	12.3	16.7	0	25.05	335.67	1493.1	12.3	0.04	43.0	17.8	60.7	14.0	96.4
UA17A-15 H(0)-4.5-2	2.67	17.25	12.3	16.7	0	60.65	812.71	3615.1							
UA17A-16 H(0)-4.5-3	2.67	17.2	12.3	16.6	0	43.18	578.612	2573.8							
UA17A-17 A(65)-36.5-1	2.67	37.03	56.9	77.1	65	60.12	805.608	3583.5	56.2	0.72	58.9	2.8	60.9	63.7	67.4
UA17A-18 A(65)-36.5-2	2.67	36.8	56.2	76.2	65	60.88	815.792	3628.8							
UA17A-20 A(65)-36.5-4	2.67	36.56	55.5	75.2	65	55.64	745.576	3316.5							
UA17A-21 A(58)-46.1-1	2.67	45.95	87.6	118.8	58	112.69	1510.046	6717.0	87.9	0.24	121.2	8.9	130.5	99.7	148.0
UA17A-22 A(58)-46.1-2	2.67	46.06	88.0	119.4	58	120.49	1614.566	7181.9							
UA17A-23 A(58)-46.1-3	2.67	46.06	88.0	119.4	58	130.47	1748.298	7776.8							
UA17A-24 A(58)-51.7-1	2.67	50.37	105.3	142.7	58	119.79	1605.186	7140.2	105.6	0.25	128.5	9.8	139.2	119.7	158.0
UA17A-25 A(58)-51.7-1	2.67	50.48	105.7	143.4	58	139.15	1864.61	8294.2							
UA17A-26 A(58)-51.7-1	2.67	50.46	105.7	143.2	58	126.58	1696.172	7544.9							

Note: Colors in the table represent the magnitude of the individual entry with green being the lowest values and red being the highest values within a column.

Dr. Narayan Yoganandan¹⁶ studied numerous tests of skull fractures from 1949-2004. The study looked at the peak forces resulting in skull fractures and how testing had led to HIC standards based upon cadaver testing. Table 7 shows the results of the Gurdjian tests that were conducted by dropping cadaver skulls onto steel plates. The Gurdjian data show that skull fractures at various locations on the skull resulted from impact KE values ranging from 948.3 J \pm 120.1 to 652.6 J \pm 67.6 J (699 ft-lbs \pm 88.6 ft-lbs to 481.3 ft-lbs \pm 49.9 ft-lbs). While the contact areas of the Gurdjian tests were not precisely documented, the contact areas are certainly higher than those of small debris fragments, which leads to dramatically different energy results than those shown in the RCC standards. The sUAS collision tests conducted at NIAR shown in Table 6 resulted in

¹⁶ Yoganandan, N, Pintar, F., Biomechanics of temporo-parietal skull fracture, *Clin Biomech (Bristol, Avon)*. 2004 Mar;19(3):225-39.

impact KEs substantially lower than those impact KEs required to obtain skull fractures during the Gurdjian tests even at the low end of the standard deviation of the mean. Furthermore, Yoganandan reported that the type and shape of the contactor significantly affected the peak force required to cause a skull fracture.¹⁶ “For the rectangular impactor, the parietal region was selected as the impact site. The mean fracture for rectangular plate impacts was 12390 N (± 3654). The average fracture force for both impact sites with the circular impactor was 5195 N (± 1010). Stiffness was computed as the average slope of the force–displacement curve between 4 and 12 kN for the rectangular plate impactor and 2–6 kN for the circular plate impactor.... The contact area of the impactor significantly affected peak forces. Hodgson and Thomas (1971) and Yoganandan et al. (1993, 1991a, 1989, 1991b) advanced similar conclusions on facial bone structures in experimental studies in 1970s and 1980s.”¹⁶ A similar result can be found in a later report by Yoganandan¹⁷ that used a 48 mm (1.9 in) radius hemispherical anvil impactor to study skull fracture. Yoganandan found dramatically lower energy levels than those reported by Gurdjian as shown in Table 7 using the hydraulic anvil with a small, radial contact area. While these tests give more credence to the RCC standards in terms of impact KE, the results are likely due to the stiffness and size of the steel hydraulic ram that imparts contact loads more like falling projectiles than those of a flexible and frangible sUAS with breakaway camera structures and plastic airframe structures or foam. The mean forces for the static and dynamic forces shown in the Yoganandan tests¹⁷ resulting in skull fracture shown in Table 8 are higher than the largest resultant force recorded during the NIAR drop tests with a flexible Phantom 3. The smallest dynamic force for all regions tested resulting in a skull fracture was 8,809 N (1,980 lbf). This gives credibility to the assessment that the Phantom 3 impacts would not have resulted in skull fractures and the subsequent low HIC and AIS results shown in the study are valid despite the higher impact KEs of the Phantom 3. The Yoganandan results give credence to the high PoF if one solely looks at impact KEs shown in Table 8. However, the resultant forces ultimately lead to a different conclusion due to the difference in character of a steel hydraulic ram contactor when compared to a flexible plastic Phantom 3.

¹⁷ Yoganandan, N, Pintar, F., Sances Jr., A., Walsh, P., Ewing, C., Thomas, D., Snyder, R., Biomechanics of Skull Fracture, *Journal of Neurotrauma*, 1995, Volume 12, Number 4, 659-668.

Table 7 –Biomechanical Data for All Skull Fractures from Gurdjian¹⁶

Biomechanical data from the Gurdjian et al. study for all fractures		
Region	Velocity (m/s)	Energy (N m)
Anterior parietal	5.8 ± 0.5	948.3 ± 120.1
Posterior parietal	5.6 ± 0.5	910.9 ± 219.0
All parietal regions	5.8 ± 0.5	943.0 ± 161.3
Mid frontal	4.6 ± 0.3	678.0 ± 156.1
Occipital	4.9 ± 0.4	652.6 ± 67.2
Anterior parietal	5.5 ± 0.8	963.3 ± 180.7
Posterior parietal	5.6 ± 0.2	833.1 ± 68.1
All parietal regions	5.3 ± 0.4	858.4 ± 54.9
Mid frontal	4.8 ± 0.4	773.7 ± 275.7
Occipital	4.8 ± 0.2	700.9 ± 28.8

Table 8 –Biomechanical Data of Skull Fracture Tests using a 48mm radius Hydraulic Anvil

ID	Loading rate (m/s)	Force (N)	Deflection (mm)	Stiffness (N/mm)	Energy (J)	Pathology
1	0.002	4464	9.1	790	18.88	Linear fracture—left temporal and parietal bones
2	0.002	5292	8.9	695	18.57	Linear fracture—orbital roof
3	0.002	5915	7.8	1143	14.07	Linear fracture—parietal, temporal, zygomatic bones
4	0.002	6182	15.4	487	44.72	Depressed fracture—inferior parietal, temporal bones
5	0.002	4642	14.1	467	36.28	Multiple depressed fracture—frontal bone
6	0.002	11898	16.6	1290	68.47	Circular fracture—lambdoid suture
7	7.2	14034	5.72	4798	31.46	Linear fracture—vertex to right orbit, frontal bone
8	7.1	13600	4.01	5867	23.51	Multiple fracture—frontal bone, LeFort III
9	7.6	13579	7.40	2540	40.00	Multiple fracture—through vertex, frontal, temporal bones
10	7.3	10009	9.74	2462	43.48	Circular fracture—superior to lambda
11	7.8	8809	3.44	4078	15.59	Multiple fracture—parietal bone, bilateral
12	8.0	11595	4.56	4394	14.06	Circular fracture—vertex region
Mean (1–6)		6399	12.0	812	33.5	
SE		(± 1134)	(± 1.6)	(± 139)	(± 8.5)	
Mean (7–12)		11938	5.8	4023	28.0	
SE		(± 885)	(± 1.0)	(± 541)	(± 5.1)	

As an extension of this analysis, the team looked at simple ways to develop a new impact KE threshold based upon the resultant force methodology introduced in this analysis. If one were to use the lowest resultant force threshold for skull fractures based upon Dr. Yoganandan’s work and the NIAR drop tests data, how could this resultant force be translated into an upper bound for a Phantom 3 in terms of impact KE that is easily testable using ballistic analysis. To this end, the team reviewed data for KE and the resultant load data to look for consistency across the set of data and the variability of the data as shown in Table 6. The table shows that the variability of the resultant load data and the corresponding 98% confidence (3 sigma) resultant load data for

the NIAR test points conducted with the Phantom 3. The trend line for the 98% confidence data points is compared with a linear trend line of the NIAR data as well as the trend line developed from the calculation of impulse force developed for bird strikes by McNaughton.¹⁸ McNaughton developed a relationship for impulse force (P_i) as a function of mass of the bird (m) and velocity (V) of the aircraft as shown below where mass is in kilograms and velocity is in knots.

$$P_i = 1.18 \times m^{2/3} \times V^2 \quad \text{Equation 1}$$

Load factors are calculated by taking the calculated impulse for the Phantom 3 using the equation above and dividing by the weight of the head (10 lbs) to determine the load factor in g's. The comparison of the trend lines for the impact KE and the resultant load factor at the head correlates well with the exception of the horizontal impact tests. Since these values fall below the maximum resultant impact load from the Yoganandan work, these values are seen as acceptable within the trend of the analysis. It is likely that a horizontal power flight curve must be segregated from the power off ballistic curves when more horizontal impact data becomes available. This trend correlates with the terminal velocity data vs. propelled data shown in Table 5. It is realistic that flight over people will not involve horizontal powered flight at the same height as non-participants, but rather more vertical impacts whether powered or unpowered.

The results of the analysis of resultant load factor versus impact KE is shown in Figure 9. The 98% confidence level (three σ) trend line is used to extrapolate the maximum impact energy for skull fractures as a function of impact KE and the intersection of the maximum load factor based upon Yoganandan shows the maximum KE value of 128 ft-lbs. The 98% confidence level threshold uses the equation for the three s linear fit of the data to calculate the resultant load factor and the load factor must always remain less than 198 g. The equation is as follows:

$$\text{Resultant Load Factor (g)} = 1.5441 * \text{impact KE (ft - lbs)} \quad \text{Equation 2}$$

The impact KE is derived from the ballistic analysis for the vehicle configuration under evaluation and the resultant load factor is calculated.

¹⁸ McNaughtan, I. I.: The Design of Leading Edge and Intake Wall Structure to Resist Bird Impact. Royal Aircraft Establishment Technical Report 72056, 1972.

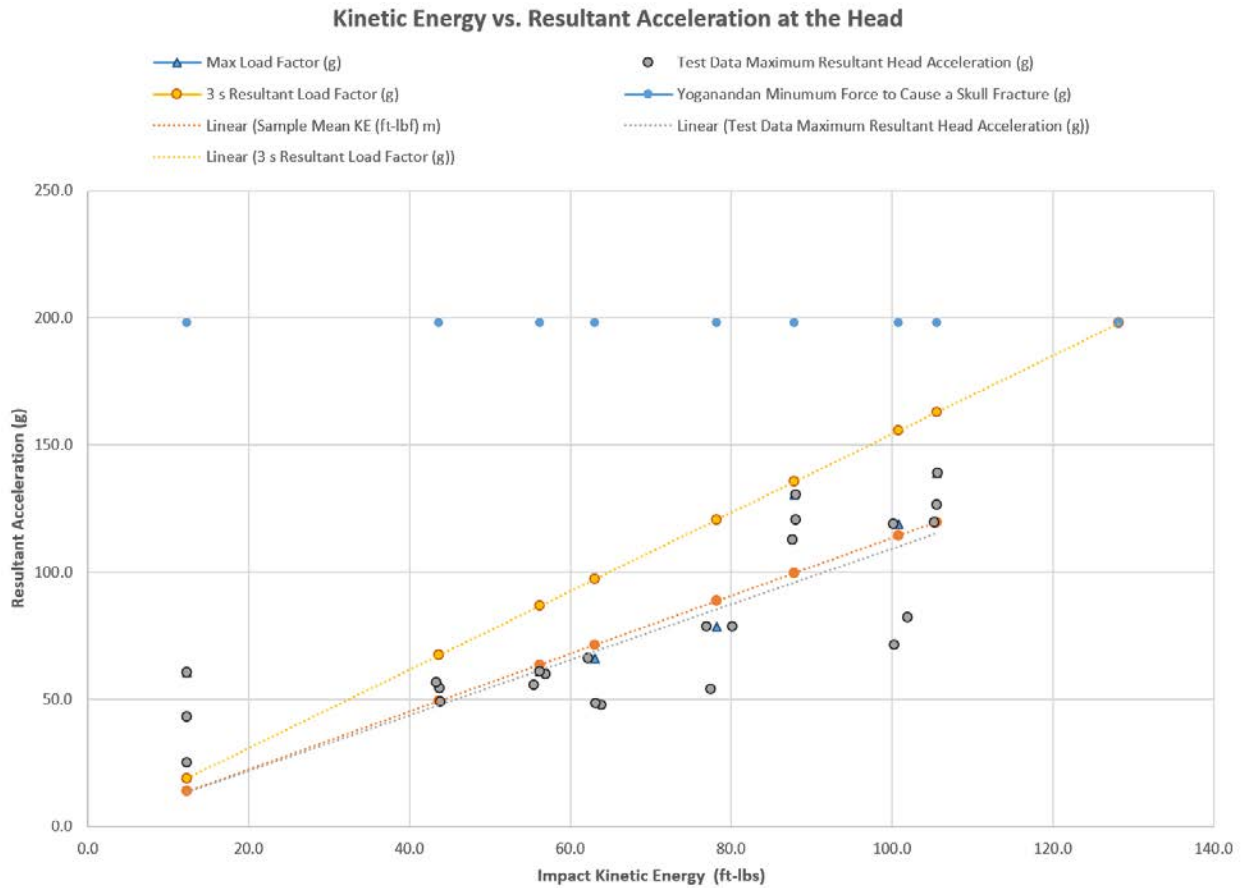


Figure 9 - Analysis of Resultant Impact for Skull Fractures versus Impact KE

To extend this analysis, the skull fracture resultant load must be applied to the metrics for neck injury and AIS3 injuries to verify that this level of resultant does not cause a neck injury that would exceed the 30% chance of an AIS3 or greater injury. The trends in the data from the NIAR drop tests shown in Table 3 and Figure 10 indicate that the impact KE required to cause head injury may not be the limiting factor in terms of impact KE relative to less than a 30% probability of an AIS3 or greater injury. Neck injury values shown in the limited NIAR tests indicate that neck injuries may be of greater concern than skull fracture. The limits imposed by the slope of the trend line for the three sigma values up to the lower bound of the Yoganandan skull fracture loads of 8,809 N or 1980 lbf resulting from 128 ft-lbs of impact KE will remain below the 30% probability of an AIS3 or greater neck injury based upon the limited data collected during these test as shown in Figure 10.

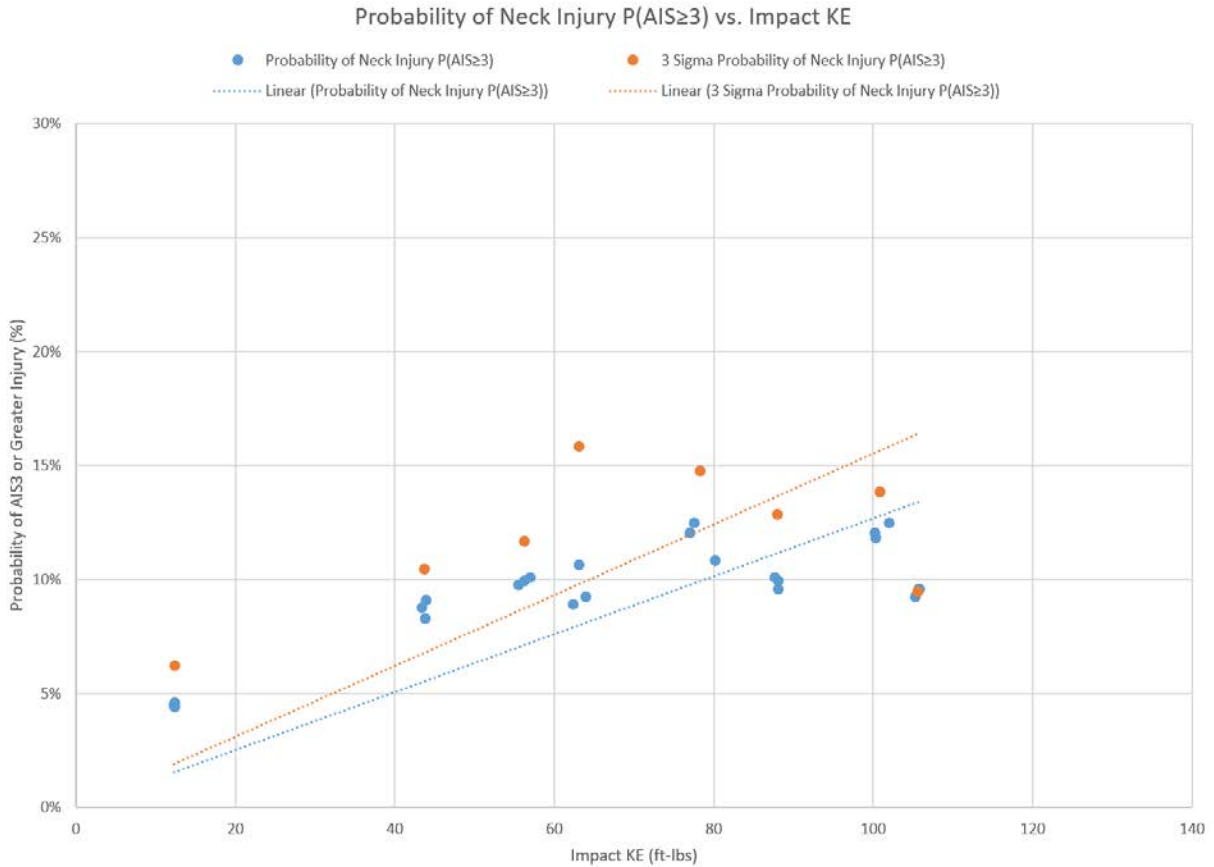


Figure 10 - Probability of Neck Injury Trends from NIAR Test Data

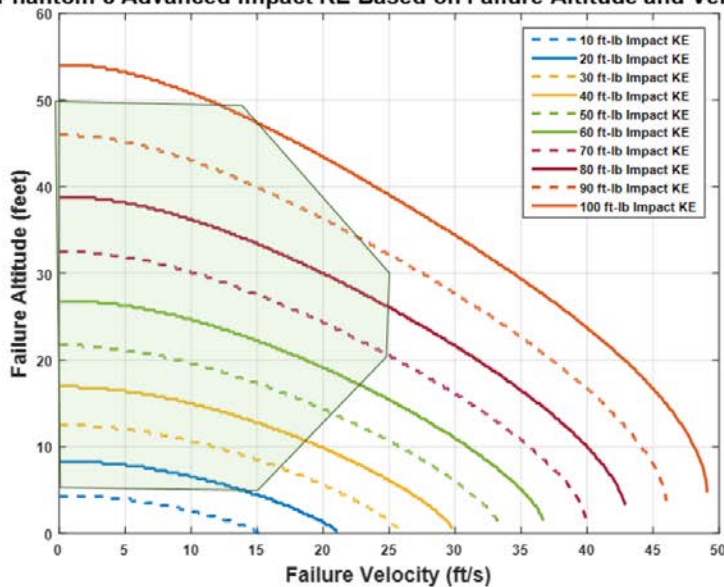
The trend lines shown in Figure 9 and Figure 10 indicate the neck injury data and head injury trends for the flexible Phantom 3 Standard and Advanced aircraft would not result in skull fractures or neck injuries for the proposed flight envelope provided in the Appendix A Part 107 waiver. The envelopes are shown in Figure 11. Using the RCC standards for impact KEs of 106 ft-lbs for the envelope proposed in the waiver and the 128 ft-lbs maximum impact KE threshold for the 98% confidence level resultant load would have resulted in a 98-100% PoF value using the RCC standards for head or thorax injury as shown in Figure 6 and 75-80% PoF values if using the area weighted and average human orientation chart shown in Figure 8 from the RCC standards. This significant gap in perceived level of safety between the RCC standards and the substantially different injury metrics observed during the drop tests suggests the RCC data does not represent the collision dynamics and injury mechanics representative of collisions with flexible, plastic sUAS platforms.

As long as the resultant load factor remains below 196 g, then there is a 98% confidence that no skull fractures will occur and there will be less than 30% probability of having a neck injury exceed AIS3 or greater. The limit of this analysis is for multi-rotor vehicles made with plastic,

flexible structures. The analysis applies to blunt force trauma type injuries. Laceration and penetration injuries must be addressed separately.

These standards are extremely conservative. The NIAR drop tests were worse case collision scenarios with no blade guards and near center of mass collisions. During a few of the tests, the impacts were slightly offset by no more than an inch, yet the offset collision caused the vehicle to roll away from the ATD dummy quickly, which resulted in a significant reduction in impact KE over other tests at the same condition. This condition was very evident in the horizontal impact tests. The three horizontal impact tests were all conducted at 12.3 ft/s; however, the resultant load at the head of the ATD dummy for the three tests was 25.05g, 60.65g and 43.18g, respectively. The variation in the first two tests can be seen in the video of the first test that had a slight offset and resulted in the Phantom 3 rotating across the head as one arm struck the head before the other and started the vehicle rotating away from the head. The other two tests had a more center of mass impact between the arms of the vehicle resulting in more energy transfer. The likelihood of less severe offset collisions is increased with the additional of blade guards, landing gear and the breakaway features of the payload for the Phantom 3.

Phantom 3 Advanced Impact KE Based on Failure Altitude and Velocity



- DJI Phantom 3 Standard:
- 1) Modified Prop Guards Installed
 - 2) Blades Parallel to Arms
 - 3) Gross Weight of 2.83 lb
 - 4) Lateral Planform = 0.313 ft²
 - 5) Vertical Planform = 0.657 ft²
 - 6) Average C_{d,vert} = 1.124
 - 7) Average C_{d,lat} = 1.122

Phantom 3 Advanced (3.01 lbs)					
#	Alt. (ft. AGL)	V Fail (ft/s)	V Impact (ft/s)	KE (ft-lb)	Impact Angle (deg.)
1	55	0	45.29	95.95	90
2	55	17	47.59	105.94	80
3	35	25	43.21	87.35	64
4	25	25	38.63	69.80	60
5	10	15	21.70	22.03	56
6	10	0	16.16	12.21	90

Figure 11 - Phantom 3 Advanced Waiver Request Envelope

Increasing the threshold of impact KE to 128 lbs for sUAS platforms for flight over people has the additional effect of dramatically increasing the operational envelope for unmanned platforms other than multi-rotors when using parachutes as safety mitigations for flight over people and

flight over heavily populated areas. Task A4 looked at the impact of parachutes with various levels of safety defined by RCC standards. While the Phantom 3 envelope shown in Figure 11 does not require a parachute to meet the 98% confidence level KE threshold of 128 ft-lbs, the use of parachutes as mitigations for blunt force trauma injuries while flying over people is critical to opening up the envelope for more robust commercial vehicles during flight over populated areas. The parachute standards reviewed in Task A4 are reevaluated in comparison to the 98% confidence level impact KE threshold of 128 ft-lbs based upon the injury metrics in this report for skull fracture and less than a 30% chance of a neck injury resulting in an AIS or greater injury. The 28 ft-lbs impact KE value from the RCC standards represents the 1% PoF of head injury and 10% probability of a thorax injury as shown in Figure 6. The use of the new metrics not only makes it possible for the Phantom 3 to be safe during Category 4 Performance Standards as defined by the Micro-ARC Final Report, but many other platforms could meet these standards at substantially higher takeoff weights using parachutes and automatic deployment mechanisms as mitigations for Category 3 and Category 4 Performance Standards. Parachutes used as safety devices in this manner must meet specific standards and provide sufficient altitude to decelerate to the speeds shown in Table 9. It is important to note that 18.0 ft/s is assumed to be the lowest reliable rate of descent that can be achieved with a parachute recovery system. Below this rate of descent, it is questionable whether there is sufficient dynamic pressure to maintain a fully inflated canopy to support deceleration of the vehicle.

Table 9 - Comparison of RCC Standards vs. Modified Impact Energy Thresholds for Various Aircraft Weights when Descending under Parachute.

Descent (fps)	Descent Velocities (kts)	Weight (lbs) Based upon RCC Standards of 28 ft-lbs impact KE (1% PoF due to Head Injury or 10% PoF due to Thorax Injury) while Standing RCC	Weight (lbs) for a 128 ft-lbs impact KE Threshold (based upon sUAS impact test with 98% confidence of no skull fracture and less than 30% chance of an AIS3 or greater injury)
14.0	8.3	9.2	42.0
16.0	9.5	7.0	32.2
18.0	10.7	5.6	25.4
20.0	11.8	4.5	20.6
22.0	13.0	3.7	17.0
24.0	14.2	3.1	14.3
26.0	15.4	2.7	12.2
28.0	16.6	2.3	10.5

2.5. Energy Transfer Analysis

The planned technical approach for the analysis of energy transfer from the Phantom 3 to the ATD dummy was initially based on the Conservation of Angular Momentum (COAM); however, the test data from NIAR was not complete enough for conducting this analysis. In lieu

of COAM analysis, the NIAR test data was used to calculate energy transfer to the dummy by way of the measured impulse (lbf-s) at the base of the head and measurement of the rotational energy of the dummy head after impact. The trends in calculated energy absorption data are logical; however, the area requires additional work, in the form of finite element analysis (FEA) simulations to fully understand the mechanics of energy transfer and dissipation through non-conservative mechanisms like losses in deformation and the differences between the results of high energy vertical and angled impacts.

The energy transfer analysis centered on evaluating the energy transfer to the ATD dummy's head during impact through the ATD's load cells and accelerometers. Before discussing this analysis in a detailed manner, it's necessary to provide an overview of the energy loss mechanisms that dissipate UAS impact KE. First, the UAS fuselage and payload deform by flexing and, in some cases, breaking. Appendix B - NIAR Test Article Damage contains a discussion of the impact damage found on each vehicle after testing. The deformation energy cannot be calculated from the available test data. The vehicle also rebounds off the ATD head and has linear and rotational velocities after impact. The energy of the rebounding aircraft is referred to as Post-Impact UAS KE. The Post-Impact UAS KE in this analysis is estimated by analyzing photometric data to determine the Phantom 3's resultant velocity and rates of rotation immediately after the vehicle breaks contact with the ATD head after impact has occurred. The impact of the UAS on the ATD head results in impulse, which is measured at the upper neck load cell. In this analysis, the energy that creates that impulse is called Transferred Energy ($E_{\text{transferred}}$). The impact, which is characterized by the impulse, results in a change in the KE of the dummy's head. The KE of the dummy's head, after the impact, is denoted as KE_{head} . The last way in which the UAS impact energy is dissipated is through direct absorption by the ATD head material, or in the case of an impact with a human head, the skull, brain, and other tissues of the head. E_{absorb} is the key parameter that relates directly to the injury potential of an impact.

The upper neck load cell measurements were used to calculate the impulse experienced by the dummy's head. Impulse, J , is the integral of a force, F , over the time interval, t , that the force acts on a mass.

$$J = \int_{t_1}^{t_2} F dt \quad \text{Equation 3}$$

In turn, the energy transfer that yielded that impulse can be calculated by the expression:

$$E_{\text{transferred}} = \frac{J^2}{2m} \quad \text{Equation 4}$$

where the mass value is based upon the weight of the ATD Dummy head of 10 lbs. The NIAR data included upper neck load cell measurements of force in the dummy head x, y, and z-directions as a function of time during the tests (Figure 12). The ATD dummy load cells measure force at 20kHz. Based on this, the time history of forces in the three principle directions were integrated over the time period of each test using a MATLAB© script. The integration calculates the area between the force curve and the x-axis (time) for the duration of the test. The

calculated impulse values are vector quantities, because they have a magnitude in terms of lbf-s and a direction based on the axis to which the force values are correlated. The total impulse measured at the upper next load cell is the vector sum or magnitude of the impulse in the x, y, and z-directions.

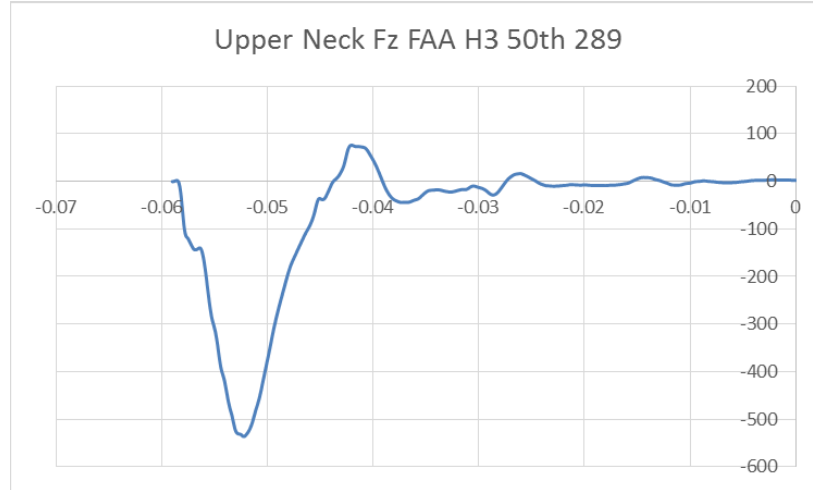


Figure 12 Time History of Upper Neck Z-direction Force During a NIAR Drop Test

The KE_{head} values used in this analysis only account for the change in head rotational energy during the collision, as the data set didn't contain enough information to determine the head's KE due to linear translation independent of rotation. The ATD head KE is given by:

$$KE_{head} = \frac{1}{2}I(\omega_2^2 - \omega_1^2) \quad \text{Equation 5}$$

where I is the mass moment of inertia of the dummy head and ω is the rotational rate of the head. Total rotational energy was taken as the sum of rotation energy about the x, y, and z axes during the impact. Based on a CAD model of the ATD Hybrid III 50th percentile male crash dummy, the mass moments of inertia used in these calculations were 0.0183, 0.0231, and 0.0107 kg/m² about the x, y, and z axes, respectively.¹⁹ These are the mass moments of inertia about the CG of the ATD dummy head.

The energy absorbed by the head is determined by the relationship:

$$E_{absorb} = E_{transferred} - KE_{head} \quad \text{Equation 6}$$

In this analysis, the absorbed energy calculations are conservative in nature, because they only include the rotational KE of the head. The estimated energy absorption values would decrease

¹⁹ Correspondence from Xianping Du, Ph.D. Student under Dr. Feng Zhu at Embry-Riddle Aeronautical University, dated 16 August 2016

with the inclusion of KE due to linear velocities, for example vertical translation of the head and body, independent of rotation, in the vertical drop impacts.

Table 10 shows the UAS Impact KE, energy transferred to the head due to impulse load ($E_{\text{transferred}}$), and the amount and percentage of the impact KE that was NOT transferred to the head. This data shows a trend in which an increasing percentage of the impact KE is not transferred to the head as the drop height and, consequently, impact velocity and KE increase. It is likely that more of the impact energy is dissipated in the distortion and flexing of the aircraft as the impact KE increases. This follows damage trends which are detailed in Appendix B - NIAR Test Article Damage. Physical inspection of thirteen of the twenty-four Phantom 3 Standard test articles showed increasing levels of damage that correlate directly to the drop height and impact velocities. Assessing the damage to the payloads of the remaining aircraft was done by viewing the impact videos. Video analysis was also used to assess whether cameras broke during testing or if they broke off during handling and shipping to UAH. The 20 ft drops resulted in either no damage to the fuselage at all or slight buckling where the vehicle arms merge into the body. None of the 20 ft drops resulted in separation of the camera or discernable damage to the camera. The 50 ft drops are characterized by damage which includes complete separation of the camera from the fuselage in one test, damage to the camera itself, significant buckling of the fuselage where the arms merge with the body, and cracking of internal supports that surround the battery. The drops from 30 and 40 ft resulted in intermediate levels of damage. The angle impact drops were characterized by increasing levels of camera damage as the impact velocity and KE increased. The 36.5 ft, 65° angle impact drops resulted in some camera damage and only one partial separation of the camera. The 51.7 ft, 58° angle drops all resulted in separation of the camera and greater degrees of damage to the aircraft. Energy dissipated through deformation and elastic energy of the Phantom 3 and other sUAS requires further investigation through FEA simulation to more precisely understand UAS impact KE loss/conversion with detailed energy absorption analysis.

Table 10 - Differences in Impact KE and Energy Transferred to ATD Head

Test Name	UAS Impact KE (ft-lb)	Energy Transferred (ft-lbs)	Difference (ft-lb)	% Impact KE Not Transferred
V(90)-20-1	34.57	24.23	10.34	29.90%
V(90)-20-2	34.96	23.72	11.24	32.14%
V(90)-20-3	34.99	23.73	11.26	32.17%
V(90)-30-1	57.47	31.16	26.31	45.78%
V(90)-30-2	57.98	31.97	26.01	44.86%
V(90)-30-3	58.54	29.06	29.48	50.36%
V(90)-40-1	64.88	33.52	31.36	48.33%
V(90)-40-2	67.31	34.43	32.88	48.85%
V(90)-40-3	78.72	35.18	43.55	55.32%
V(90)-50-1	90.02	40.15	49.87	55.40%
V(90)-50-2	86.62	39.63	46.99	54.25%
V(90)-50-3	84.42	39.33	45.09	53.41%
H(0)-4.5-1	11.90	7.36	4.53	38.11%
H(0)-4.5-2	11.61	4.23	7.38	63.55%
H(0)-4.5-3	10.33	4.17	6.16	59.62%
A(65)-36.5-1	46.06	24.42	21.64	46.98%
A(65)-36.5-2	48.45	24.18	24.28	50.11%
A(65)-36.5-4	50.65	22.24	28.40	56.09%
A(58)-46.1-1	78.64	28.48	50.16	63.79%
A(58)-46.1-2	84.72	28.15	56.57	66.77%
A(58)-46.1-3	77.76	26.96	50.80	65.33%
A(58)-51.7-1	96.33	26.37	69.96	72.63%
A(58)-51.7-2	100.57	27.59	72.98	72.57%
A(58)-51.7-3	99.15	26.78	72.37	72.99%

Table 11 shows the UAS Initial KE, $E_{\text{transferred}}$, KE_{head} , and E_{absorb} values calculated for each test. The calculated energy transfer shows that impulse increases as drop altitude increases. Because the impact in the first twelve tests was vertical and aligned closely with the ATD head's CG and there is little energy that results in rotational motion of the head. The angle-impact tests are marked by generally higher KE_{head} values, in particular the 46.1 ft, 58° and 51.7 ft, 58° drops. The angled impacts had less energy transferred to the head as the camera and payload struck the front of the head and slid down the forehead and nose of the ATD dummy as the camera and camera mount broke away prior to contact of the body of the Phantom 3. Furthermore, the neck is much more capable of extension than compression and more of the energy transferred to the head resulted in translation of the head that could not occur during compression of the neck in the vertical tests. Based on the greater KE_{head} values in the angled impact tests, the 46.1 ft, 58° and 51.7 ft, 58° angle impact drops are characterized by lower percentages of energy absorbed by the head. It can be concluded that the head, while undergoing greater accelerations, will absorb less of a blunt impact when it is free to move and when the UAS does not have a complete center of mass contact due to an offset or interaction of some component of the vehicle (such as the payload) that results in the breakaway of a frangible component or the interaction of a portion of the aircraft that deflects the vehicle from creating a direct contact. An average of 50% of the UAS impact KE becomes E_{absorb} across all of the vertical drop tests. The magnitude

of absorbed energy increases, which follows a trend of increasing HIC15 values calculated by NIAR. HIC15 is a measure of the likelihood of a head injury arising from an impact. The maximum tolerable value of HIC15 is 700.⁶ At worst, the angle impact tests that drop from 51.7 ft only achieve 24% of the maximum tolerable value for HIC15. The fact that this analysis shows low percentages of the UAS impact KE being absorbed by the head correlates well with the low likelihood of AIS-3 or greater injuries (Table 3) and the low HIC15 values from the tests.

Table 11 - Impact Energy Absorption by the ATD Dummy Head and Injury Metrics

Test Name	UAS Impact KE (ft-lb)	Transferred Energy (ft-lbs)	KE Head (ft-lb)	Energy Absorbed by Head (ft-lbs)	% Impact Energy Absorbed	HIC Value (Max 700)
V(90)-20-1	34.57	24.23	1.91	22.33	64.58%	7.83
V(90)-20-2	34.96	23.72	9.06	14.67	41.95%	29.18
V(90)-20-3	34.99	23.73	0.25	23.48	67.10%	19.94
V(90)-30-1	57.47	31.16	0.17	31.00	53.93%	12.01
V(90)-30-2	57.98	31.97	0.29	31.68	54.64%	14.99
V(90)-30-3	58.54	29.06	0.10	28.96	49.48%	15.64
V(90)-40-1	64.88	33.52	1.14	32.38	49.90%	19.26
V(90)-40-2	67.31	34.43	0.75	33.68	50.04%	23.45
V(90)-40-3	78.72	35.18	0.38	34.80	44.20%	23.02
V(90)-50-1	90.02	40.15	0.36	39.79	44.20%	46.62
V(90)-50-2	86.62	39.63	0.29	39.34	45.42%	34.13
V(90)-50-3	84.42	39.33	0.62	38.72	45.86%	42.79
H(0)-4.5-1	11.90	7.36	0.61	6.75	56.72%	59.54
H(0)-4.5-2	11.61	4.23	0.35	3.89	33.47%	48.04
H(0)-4.5-3	10.33	4.17	0.17	4.00	38.69%	42.24
A(65)-36.5-1	46.06	24.42	1.28	23.14	50.24%	39.55
A(65)-36.5-2	48.45	24.18	0.17	24.00	49.54%	30.25
A(65)-36.5-4	50.65	22.24	0.50	21.74	42.93%	26.25
A(58)-46.1-1	78.64	28.48	6.44	22.04	28.02%	107.94
A(58)-46.1-2	84.72	28.15	10.32	17.83	21.04%	119.7
A(58)-46.1-3	77.76	26.96	8.68	18.28	23.50%	147.82
A(58)-51.7-1	96.33	26.37	13.54	12.83	13.32%	137.17
A(58)-51.7-2	100.57	27.59	16.04	11.55	11.48%	165.07
A(58)-51.7-3	99.15	26.78	15.99	10.79	10.88%	123.64

The COAM approach was originally selected because the dummy is a set of masses connected by hinges. The hip hinge was assumed to be fixed, and therefore angular momentum of all masses in the collision could be conserved around that point, i.e. the net angular momentum about the hip hinge is always equal to zero. As such, the angular momentum of the Phantom 3/dummy system prior to the impact is equal to that of the Phantom 3 dummy system after the impact. Appendix A explains COAM and its application to this system in greater detail with diagrams and equations. Strict Conservation of Momentum could not be applied because the dummy was not free to translate.

After reviewing the NIAR test data and processing the data available to determine energy and momentum values during each test, it was determined that the data was not capable of fully supporting the COAM analysis. The dummy head z-axis linear motion was not measured in the photometric data. The dummy's torso moved during impacts, but the photometric data did not include torso linear motion and rates of rotation. During post-processing, it was not possible to calculate position vectors from the dummy's hip hinge to the Phantom 3, head CG, and torso CG from the NIAR dataset. These portions of data are an essential part of calculating angular momentum contributions based on the motion of masses. Alternatively, researchers attempted to calculate component velocities and displacements during impacts from head accelerometer data and time stamps; however, the resulting values were exceedingly low. There were inconsistencies in the estimated vehicle rotational and translational KE following impact, for example, during Test UA17A-11 V(90)-50-1. The photometric data from these tests showed that the vehicle had between 6-12 times the amount of rotational energy than what was observed in Tests UA17A-12 V(90)-50-1 and UA17A-13 V(90)-50-3. This difference was not observed in the number of complete or partial vehicle rotations after the impact recorded in videos of the three tests. Impact energy expended during vehicle deformation (elastic and plastic) and payload damage cannot be accounted for through COAM analysis. Additionally, the evaluated Phantom 3 total post-impact KE had high outlier values in tests 20-1, 30-2, 50-1, 4.5-1, 36.5-1, 46.1-3, and 51.7-3 (Table 12). Test 20-1 is particularly problematic, because it shows that 32.66% of the UAS Impact KE remains as Post-Impact KE, which conflicts with analysis showing that 70% of the UAS Impact KE is experienced as impulse at the base of the head. The inconsistencies in this data served to support the conclusion that the COAM method was untenable in this application.

Table 12 - UAS Impact KE and Post-Impact KE from Photometric Data

Test Name	UAS Impact KE (ft-lb)	UAS Post-Impact KE	% Impact KE
V(90)-20-1	34.57	11.29	32.66%
V(90)-20-2	34.96	7.68	21.97%
V(90)-20-3	34.99	8.08	23.11%
V(90)-30-1	57.47	8.00	13.92%
V(90)-30-2	57.98	11.16	19.24%
V(90)-30-3	58.54	9.12	15.59%
V(90)-40-1	64.88	8.20	12.64%
V(90)-40-2	67.31	3.91	5.81%
V(90)-40-3	78.72	4.25	5.39%
V(90)-50-1	90.02	37.70	41.88%
V(90)-50-2	86.62	7.22	8.33%
V(90)-50-3	84.42	2.10	2.49%
H(0)-4.5-1	11.90	2.70	22.68%
H(0)-4.5-2	11.61	0.34	2.95%
H(0)-4.5-3	10.33	0.00	0.00%
A(65)-36.5-1	46.06	7.26	15.75%
A(65)-36.5-2	48.45	11.13	22.97%
A(65)-36.5-4	50.65	5.48	10.81%
A(58)-46.1-1	78.64	6.10	7.76%
A(58)-46.1-2	84.72	11.71	13.82%
A(58)-46.1-3	77.76	0.89	1.15%
A(58)-51.7-1	96.33	16.31	16.93%
A(58)-51.7-2	100.57	11.08	11.02%
A(58)-51.7-3	99.15	25.30	25.51%

2.6. Pendulum Testing of Blade Guards as a Laceration Mitigation

The FAA A4 Project team concluded that the most prevalent type of injuries associated with sUAS are laceration injuries from propellers through analysis of Academy of Model Aeronautics (AMA) injury records and online videos. The mitigation of laceration injuries is an essential part of managing risk for operations directly over people with a Phantom 3 multirotor aircraft. Conducting testing of the design of the blade guards to determine their resilience during a collision and verifying that the blade guards limit blade contact during horizontal impacts during a credible aircraft failure scenario under UAH's Part 107 waiver application CONOPS is critical to protecting the public when operating over people.

UAH installed the stock blade guards on the Phantom 3 aircraft and replaced the string connection between the guards with RC aircraft control rods comprised of steel clevises and carbon fiber tubes (Figure 13). The guard link prevents limbs or other objects from getting between the propellers. The string was replaced because it does not tolerate impact well and is difficult to install correctly. A solid connection between the propeller guards is essential because it prevents a limb from being pulled toward the aircraft body and trapped by counter-rotating blades.



Figure 13 - Modified blade guard link (highlighted with red oval)

UAH conducted a pendulum test in the UAH Mechanical and Aerospace Engineering Department's Autonomous Tracking Optical Measurement (ATOM) laboratory.²⁰ During vehicle tests with guards installed (Figure 13), the phantom aircraft was swung on a 14-foot pendulum at varying speeds to strike a chamois-padded PVC pipe in vicinity of the carbon-fiber blade guard link (Figure 14). The padded pipe was used as a surrogate for a human arm or other body part capable of fitting between the blade guards. The ATOM lab's motion tracking cameras were used to determine the impact velocity and track the locations of visual markers, placed on the aircraft, during an impact sequence. By placing markers on the blades and blade guards, it is possible to calculate the relative position of the markers with respect to each other and determine the extent of blade excursion beyond the guards during an impact.

²⁰ <http://www.uah.edu/eng/eng-research/research-laboratories>, accessed 08/20/2016

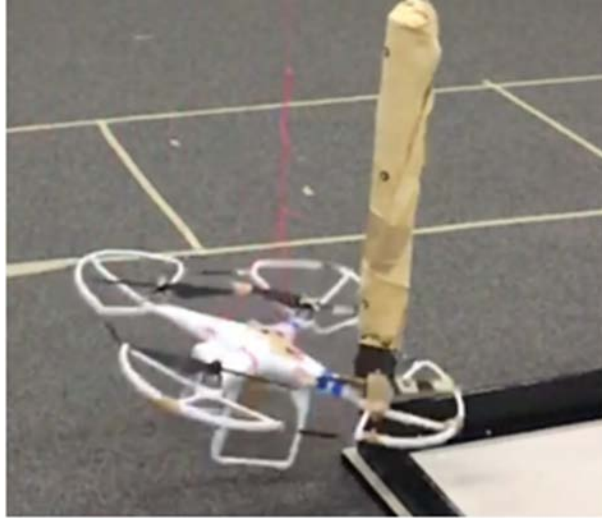


Figure 14 - Blade guard impact test

During the first seven tests, it was not easily apparent how far the blade tips extended beyond the guards during blade guard impact with the surrogate arm based on the marker setup. For the final two tests, more markers were added to the aircraft blades and the guards to clearly ascertain the amount of blade tip excursion beyond the guards. This final visual marker configuration is shown in Figure 15. Figure 15 also shows the individual marker naming convention used to annotate the positions along the left guard, connector, right guard, left/right propellers, and the Phantom's body to correlate relative positions during image capture and post-processing in the ATOM laboratory.

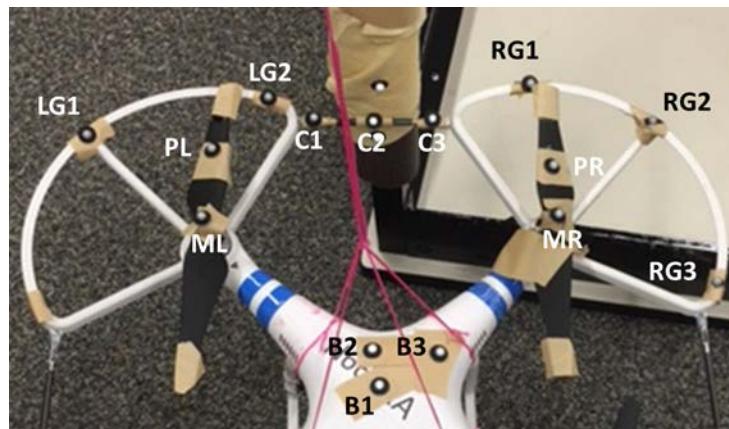


Figure 15 - Visual Marker Configuration During Tests 8 and 9

The test results are shown in Table 13. The link was damaged during an impact at close to 10 kts; however, the surrogate limb did not go between the guards. One 7 kts impact broke the guards prior to the aircraft rebounding. The fastest impact test, at 15 kts, broke the guards, but the vehicle still rebounded from the impact point. While parts of the guards broke on some tests, the outer perimeter formed by the guards and links remained intact, and the vehicle always rebounded away from the post after the collision.

Table 13 - Pendulum Test Results

Test #	Impact Speed (knots)	Limb Penetration Past Link	Blades Go Past Guards (Cutting Potential)	Remark
1	6.93	No	Indeterminant - Superficial Cutting Possible	No Damage
2	7	No	Indeterminant - Superficial Cutting Possible	No Damage
3	7	No	Indeterminant - Superficial Cutting Possible	Guard Damaged
4	9	No	Indeterminant - Superficial Cutting Possible	Connector Damaged
5	9	No	Indeterminant - Superficial Cutting Possible	Guard Damaged
6	8.95	No	Indeterminant - Superficial Cutting Possible	Connector Clevis Opened
7	9.84	No	Indeterminant - Superficial Cutting Possible	No Damage
8	7	No	Yes - Approx. 1.3 cm - Momentary Cutting	Broken Guard
9	15	No	Yes - Approx. 2.7 cm - Momentary Cutting	Broken Guard

Figure 16 shows how the guards broke during tests 8 and 9, which had impact speeds of approximately 7 and 15 kts, respectively. The image from test 8 shows that the blade guard almost completely broke, and the test 9 image shows that the post connecting the outer guard radius to the motor mount is completely broken. This indicates that any impact with a horizontal speed of 10 kts or greater will probably break the guard connections where they mount to the aircraft.

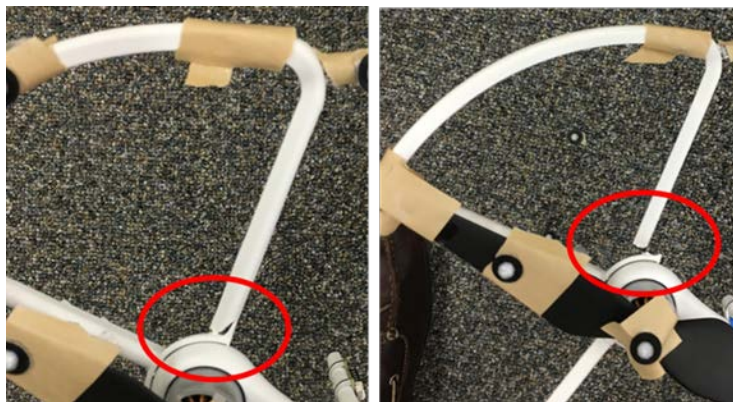


Figure 16 - Guard Damage during test 8 (left) and test 9 (right)

Tests demonstrated the blade guards had sufficient strength to prevent most cutting injuries when impact horizontal impact velocities are less than 10 kts (16.89 ft/s). The worst case condition for laceration injuries is an uncontrolled descent in which the aircraft lands in an edgewise manner

that exposes the guards to a horizontal impact velocity significantly exceeds 10 kts. In this case, a non-participant would be exposed to the blades directly or with the blade guards damaged at impact with the blades spinning. The best mitigation for laceration injuries under this scenario is for the operator to disarm the vehicle or hit a motor stop switch following loss of control.

The waiver application discussed the most probable impact angles based on ballistic characterization of the vehicle and showed the majority of impacts will occur with at least a 55° impact angle with the aircraft falling in a level attitude. The assumption of a level attitude during power-off, descending flight has been validated throughout UAH's A4 and A11 flight testing of the Phantom 2 and Phantom 3 aircraft.⁴ During an angled descent of 55° or greater, which is the most credible impact scenario, the upward component of the impact force will push the blade guard into the blades as shown in Figure 17. During a collision sequence, the blade guard will push into the blades resulting in motor stoppage on the blade closest to the contact point with the individual where the impact occurred. Figure 18 shows a simple static load test applied to the blade guard of the Phantom 2 to determine how much force is required to deflect the blade guard into the blades. This static test showed that the blade guards require a contact the blades with 2.2 lbs of upward force to deflect the blade guards into the blades. This is a low value that is likely to be exceeded during any impact.

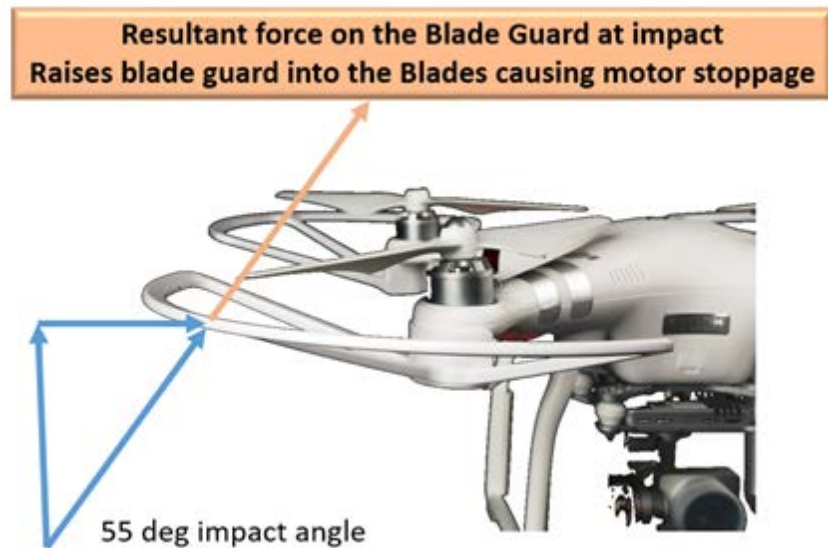


Figure 17 - Force Components on Blade Guard at 55 deg Impact Angle

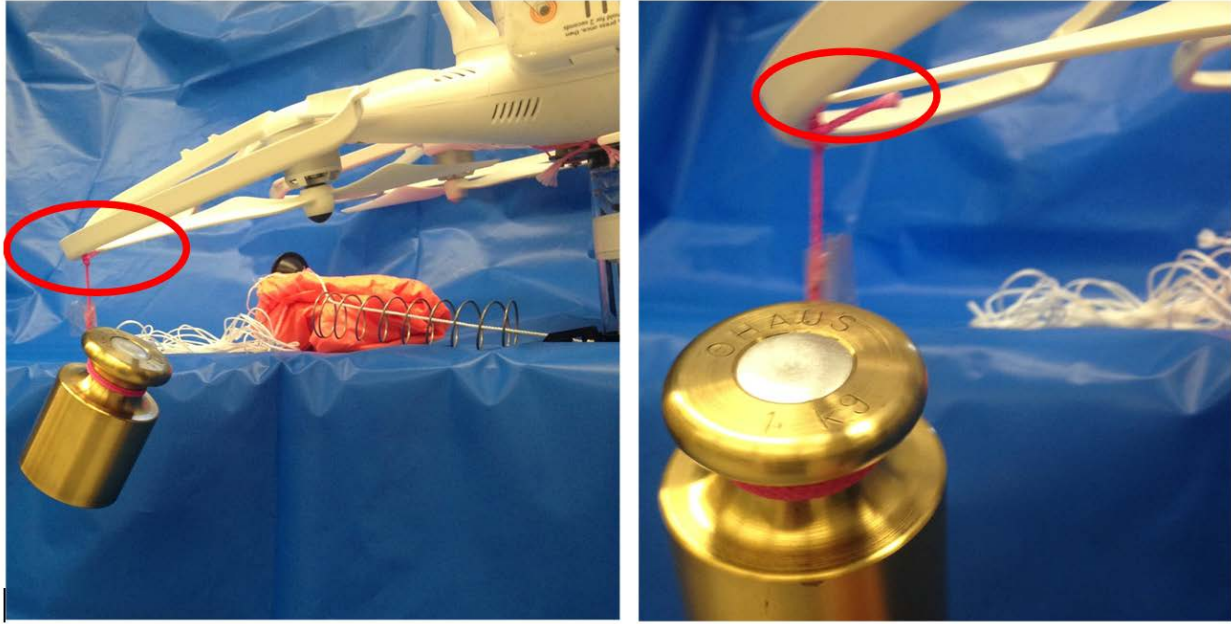


Figure 18 - Static Load Testing Showing Blade Guard Contact with the Blade Under 1kg Loading (contact is show in red oval)

3. Proposed Standards

The proposed standards are included as Appendix C and Appendix D. These two methods provide separate options for evaluating ground collision severity with people. The proposed standard in Appendix C relies purely on ballistic characterization and estimated ground impact KE correlated to RCC thresholds for injury in its analysis of potential injury severity and the following operational risk assessment. The proposed standard in Appendix D extends the assessment of potential injuries and their severity to estimated resultant impact loads for assessment of injury potential using Yoganandan's established thresholds for skull fracture and FMVSS 208 standards for neck injury against a 30% chance of AIS3 or greater injury. Both methods can be applied using test techniques and analysis readily available to the applicant or through use of an aerospace contractor without need for a specialized testing facility. Test procedures and methods are addressed specifically in the respective appendix for each one of the methods.

4. Conclusion and Recommendations

The research led to successful submission of a Part 107 waiver for flight over people that provided substantiation data to meet the Category 4 Performance Standards defined by the Micro-ARC Final Report¹. The waiver and this final report include new methodologies for determining safety thresholds other than those established by the RCC standards. The 98% confidence level resultant load standard in Appendix D is based upon drop tests data, skull fracture testing and many other references used to establish collision metrics. The Phantom 3 Standard and Advanced with modified blade guards and other multi-rotors in this class of vehicles provide different collision dynamics and different collision geometries than the small mass, large fragment, metal debris that were used to develop the PoF charts included in the RCC standards and applied to range safety for hypervelocity projectiles and missiles. Flexible, plastic vehicle structures and frangible payloads do not transfer energy during collisions in the same manner as the smaller metal debris. The Phantom 3 and other sUAS platforms remain in one piece with significant elastic response during collision with humans. The structure, landing gear and blade guards serve as flexible, compliant barriers that minimize the energy absorbed by the body, reduce the possibility of collision with the center of mass of the vehicle and minimize collision impacts with smaller areas of the body such as the thorax. The focus of the analysis addresses skull fractures and injuries to the neck area since these are the most vulnerable areas when operating over dense populations of people, especially under the operating conditions required to meet the Category 4 Performance Standards. The consideration of impact energy standards other than the RCC PoF standards for impact KE is a new approach and provides better insight into the injury mechanisms associated with sUAS ground collisions with humans. Safe operation can be conducted when operating these sUAS platforms over people and the application of the KE standards in this report extends the capabilities of safety mechanisms such as parachutes for larger platforms up to 25.4 lbs for flight over people under Category 4 Performance Standards once parachute qualification standards for this class of vehicle are better understood in terms of deceleration and vehicle dynamics required for safe deployment.

Many of these approaches are new, but the methods proposed in this research provide a solid foundation from which to continue future research for safe operation of sUAS for flight over people and provides an initial framework for clear standards for evaluating commercial platforms for future waivers required for flight over people as outlined in Appendix C and D. Laceration injuries due to blades and penetration injuries must always be addressed by the applicant, and an operational risk assessment must be completed to evaluate all the hazards and impacts that may impact safe operations when flying over people. The waiver request submitted in Appendix A provides a framework for such an assessment for flight over people. The future research areas are direct extensions of the work conducted under Task A11 and should be considered by the FAA for future funding to continue to expand safe commercial operations within the NAS.

5. Future Research Proposed to Address Research Gaps

During discussions with the FAA, it is clear that there are a number of research areas that require additional testing or require additional fundamental research to extend this effort for use in establishing regulatory standards. The following are identified by the team following the A11 research.

5.1. Dynamic Modeling of UAS for a Wider Variety of Failure Modes.

Dynamic modeling of small UAS to account for vehicle dynamics associated with a wider variety of failure modes beyond loss of power to all four motors is critical to defining a more complete safety case for flight over people. Dynamic modeling of failure modes such as loss of one or more rotors, software failures, etc. is required to determine impact angles, orientation and KE values to properly define collision impact conditions and to properly validate mitigations and vehicle characteristics as they relate to injury metrics. This work has been proposed to the FAA in 2016 in W64 – ASSURE White Paper - Falling Multi-Rotor Dynamics Study.

5.2. Blade Guard Development and Standards

Blade guards and mitigations associated with laceration injuries require additional research to develop standards for determining how these modifications best address the elimination or substantial mitigation of laceration injuries during flight over people.

5.3. Parachute Standards to Reduce Impact KEs

While parachutes can substantially reduce the impact KE during loss of control events, the development of certification standards is required to properly evaluate parachute dynamics to determine deployment, inflation and deceleration times required to mitigate impact collisions. Furthermore, this research must assess the deployment of parachutes under dynamic failure conditions when software is used to deploy the parachute and shutdown rotors as a safety mitigation. Automatic, software-driven parachute deployment is an important feature for Visual Line of Sight operations and an absolutely essential feature for Beyond Visual Line of Sight operations. The establishment of these standards could substantially open the commercial UAS in the NAS system involved in flight over people for both multi-rotor vehicles and fixed wing platforms. This work has been proposed to the FAA in 2016 in W69 – ASSURE White Paper - Standards Development for sUAS Parachute Recovery Systems.

5.4. Probability of Ground Collision with People

The analysis conducted in Task A4 and Task A11 has solely focused on the collision severity portion of the safety assessment, and little information and modeling has been conducted to determine the probability of collision with individuals on the ground when using various densities of people and a wider variety of dynamic failures that can occur with UAS under credible scenarios. The modeling will inform probability of actually hitting a person as well as determine which portions of the body are contacted such that the type and extent of injuries can be addressed analytically rather than by inference from RCC data on debris. This analysis can provide the basis for additional collision testing to refine the work conducted by task A4 and A11. This work has been proposed to the FAA in 2016 in W65 – ASSURE White Paper - Probability of UAS Ground Strike to People and Objects.

5.5. Additional sUAS Collision Tests and Development of an FMVSS 208 Like Analytical Standard

The work conducted under A11 requires additional collision data to refine the analytical techniques that can be applied to a more robust range of sUAS platforms without the requirements for extensive collision testing of sUAS platforms. The refinement of analytical methods associated with collision dynamics provides a method for applicants to analyze their vehicles against a standard using engineering methods and creating vehicles that have safe crash dynamics as a function of design.

Appendix A – UAH Part 107 Waiver Submission for Flight Over People



August 25, 2016

Ms. Sabrina Saunders-Hodge
Federal Aviation Administration
800 Independence Avenue, SW, Room 339
Washington, DC 20591

Subject: Request for Waiver to Part 107.39 Operation Over Human Beings

Dear Ms. Saunders-Hodge:

The University of Alabama in Huntsville (UAH) is seeking a waiver to § 107.39 Operation Over Human Beings for the Phantom 3 Standard and Phantom 3 Advanced to support research activities as well as collect video images for use in documenting university events. While UAH is a public university, unmanned aircraft operations under this waiver will be conducted in accordance with Part 107 as a civil operation.

The waiver request includes data and technical evaluations to substantiate safe limits for the Phantom 3 Standard and Advanced aircraft operating over people that meet the Category 4 Performance Standards outlined in the Micro Unmanned Aircraft Systems Aviation Rulemaking Committee (Micro-ARC) ARC Recommendations Final Report dated 1 April 2016. The waiver request establishes operating airspeeds and altitudes that minimize risk to the public and establish the basis for meeting the 30% or lower chance of causing an Abbreviated Injury Scale Level 3 injury or greater upon impact with a person. Furthermore, UAH has applied modifications to the unmanned aircraft and established operating limits/controls that minimize laceration injuries in the event of a collision.

All operational limits are based upon computational fluid dynamics, flight test, collision drop tests and injury metrics established by the National Highway Transportation Safety Administration. The data provided substantially improves the knowledge related to kinetic energy and blunt force trauma injury caused by UAS platforms during ground collisions over kinetic energy limits established by fragmentation data and non-lethal submunitions research typically used to establish safety cases for small unmanned aircraft systems.

We look forward the FAA's consideration and approval of this waiver request. Please direct all technical questions to the undersigned at (256) 824-6846 or email: arterbd@uah.edu.

Sincerely,

A handwritten signature in blue ink, appearing to read 'David R. Arterburn', with a stylized flourish at the end.

David R. Arterburn
Director, Rotorcraft Systems Engineering
and Simulation Center

Enclosures: 1) Waiver Request

Appendix B - NIAR Test Article Damage

B.1 Summary

Thirteen of the Phantom 3 Standard test articles that were used for drop testing by NIAR were inspected to evaluate the resulting damage to the fuselage, payload and battery. The remaining vehicles were assessed by viewing the impact video to determine if the payload separated on impact. A summary of the vehicle damage is provided in Table B - 1. This appendix also includes pictures of the damage to help qualify the information in Table B - 1. These inspections did not include methods like x-ray, non-destructive inspections or power-on testing. The most common damage seen across the tests was payload damage. The payload camera has two weak points where the camera separates from the gimbal. The damage to the fuselage occurs because of flexing and buckling during impact. In the 50 ft drop tests internal fuselage damage is observed. The batteries of the Phantom 3 test articles did not sustain any obvious physical damage like cuts, punctures, or bulging. Further battery charging and testing may be performed to ascertain if there was internal damage due to acceleration or impingement by the fuselage as it distorted during impact. The section below describes the damage to each component of the Phantom.

Table B - 1 Summary of Test Article Damage

Test Name	Description	Fuselage damage	Payload damage	Battery damage	Payload Separation in Video
UA17A-01	V(90)-20-1	No physical inspection			No separation
UA17A-02	V(90)-20-2	No damage	Cracks in the camera	No	No separation
UA17A-03	V(90)-20-3	No physical inspection			No separation
UA17A-04	V(90)-30-no test	Slight buckling	Camera breaks away	No	no video available
UA17A-05	V(90)-30-1	Very little buckling	Cracks in the camera	No	No separation
UA17A-06	V(90)-30-2	No physical inspection			broken, but intact
UA17A-07	V(90)-30-3	Very little buckling	Cracks in the camera	No	No separation
UA17A-08	V(90)-40-1	No physical inspection			Partial separation
UA17A-09	V(90)-40-2	No physical inspection			No separation
UA17A-10	V(90)-40-3	moderate buckling	partially breaks	No	No separation
UA17A-11	V(90)-50-1	Severe buckling	Cracks in the camera	No	No separation
UA17A-12	V(90)-50-2	Buckling, cracks, creases	Cracks in the camera	No	No separation
UA17A-13	V(90)-50-3	Buckling, internal cracking	Cracks in the camera	No	Partial separation
UA17A-14	H(0)-4.5-1	No physical inspection			No separation
UA17A-15	H(0)-4.5-2	No physical inspection			No separation
UA17A-16	H(0)-4.5-3	No physical inspection			No separation
UA17A-17	A(65)-36.5-1	No physical inspection			Partial separation
UA17A-18	A(65)-36.5-2	Very little buckling	Cracks in the camera	No	No separation
UA17A-19	A(65)-36.5-3No Test	Very little buckling	Cracks in the camera	No	no video available
UA17A-20	A(65)-36.5-4	No physical inspection			No separation
UA17A-21	A(58)-46.1-1	No physical inspection			Separation
UA17A-22	A(58)-46.1-2	No damage	Cracks in the camera	No	Partial separation
UA17A-23	A(58)-46.1-3	No damage	Cracks in the camera	No	No separation
UA17A-24	A(58)-51.7-1	Buckling and internal cracking	Cracked Payload Mount	No	Separation
UA17A-25	A(58)-51.7-2	No physical inspection			Separation
UA17A-26	A(58)-51.7-3	No physical inspection			Separation

B.1.1 Fuselage Damage

When the Phantom 3 impacts the dummy head, it undergoes flexing where the arms merge into the fuselage. The Phantom fuselage is comprised of the upper and lower shells and buckling between these two frames is the most commonly occurring damage. Figure B - 1 and Figure B - 2 show the most common damage on the fuselage. This damage varies from very slight buckling to severe buckling and cracking of the frame. In the angular drop tests at high speeds, the fuselage internal structure is damaged (Figure B - 3). This damage was observed only after pulling the battery out. Due to the internal damage, the battery could not be pushed back inside the fuselage. The motors on the test articles do not undergo any damage. In some test articles, the propellers are damaged and bent (Figure B - 4). This could be a result of the drops or transportation from NIAR to UAH.



Figure B - 1 - Buckling on Test Article UA17A-05



Figure B - 2 - Internal Fuselage Cracking on Test Article UA17A-24



Figure B - 3 - Significant Buckling and Cracking on Fuselage of Test Article UA17A-11



Figure B - 4 - Bent propeller on the Test Article UA17A-13

B.2.1 Payload Damage

The most noticeable and severe damage in every drop is observed at the payload. Most of the tests involve initial contact of the payload with the dummy head before any other part of the vehicle. The most common damage to the payload is observed in Figure B - 5. At this location, cracks developed in the base plate of the camera because the camera is compressed into it. Figure B - 6 shows how the camera commonly breaks away from the payload gimbal. This image shows that the motor/joint for controlling camera elevation is the weakest link on the payload where loads can lead to separation. For high impact velocities at an angle, the entire payload separates away from the test article (Figure B - 7). The payload damage can be categorized into three types, cracks at the base plate, camera separation from the gimbal and complete (camera, gimbal, and base plate) payload separation.



Figure B - 5 - Damage on Payload Base Plate on Test Article UA17A-11



Figure B - 6 - Camera Separation from Gimbal at the Elevation Motor on Test Article UA17A-10



Figure B - 7 - Complete Payload Separation in Test Article UA17A-22

B.3.1 Battery Damage

No obvious physical damage was found on any of the batteries from 26 test articles returned from NIAR following the drop tests. Damage to battery compartments was identified as shown in Figure B-2 that could have led to battery damage of contact was made with the soft sides of the batteries of the Phantom 3, but none were observed as a function of these tests.

Appendix C - Proposed Standard with Impact KE Assessment Only

C.1. Introduction

The tests and analysis conducted under Task A4 and Task A11 of the FAA UAS CoE have led to the development of a proposed standard to be used by industry to substantiate vehicle-specific operational height-velocity envelopes for safe operation for flight over people. The proposed standard uses the same methodology used to establish an envelope during Task A11.

Additionally, the standard outlines test procedures that can be conducted by the applicant that do not require use of a separate testing site or significant increase in costs or time to collect envelope validation data for part 107 waiver submission. The basic steps in the process are as follows:

- a. Develop a CONOPS.
- b. Conduct an operational safety assessment to identify hazards.
- c. Identify aircraft modifications required for mitigations for laceration and penetration injury hazards (parachutes, blade guards, material selection, frangibility, etc.).
- d. Conduct CFD analysis or other analysis to determine the flat plate drag area and mass of the applicant's proposed vehicle configuration to refine the height-velocity diagram.
- e. Conduct a ballistic analysis/characterization of the applicant vehicle based upon flat plate drag area and mass of the applicant's proposed vehicle configuration to develop initial height-velocity diagram to achieve CONOPS.
- f. Conduct flight test to substantiate the flat plate drag area and mass of the applicant's proposed vehicle configuration to refine the height-velocity diagram from the original ballistic analysis.
- g. Evaluate ground impact KE from vehicle ballistic characterization and use RCC impact KE thresholds, correlated to PoF to determine the acceptable Height-Velocity limitations for the waiver application.

C.2. Flow chart with Data Requirements

The data requirements to support this testing standard and the testing standard workflow are illustrated in Figure C-1. The applicant must provide aircraft CAD models, the CONOPS describing the operations covered by the waiver application, and the vehicle model. An initial operational safety assessment will be provided by the applicant. Depending on the availability of time, funding, software and expertise, an applicant may choose to conduct ballistic characterization via CFD flow field simulation, ballistic modeling, flight test validation, or conduct an in-depth flight test to support ballistic characterization. In the former method, the applicant or a representative organization will evaluate and modify aircraft CAD models for use in CFD simulation and then conduct ballistic characterization of the vehicle based on the vehicle

mass and aerodynamic properties. The applicant or a representative will conduct flight test following integration of the vehicle state data logging unit and procedures that are established for safe recovery of the vehicle following power-off drops from altitude. If an applicant chooses to use flight test alone, this will be used to verify the vertical flat plate drag area of the vehicle and impact KE-levels based on failure airspeed. Penetration and laceration mitigations will be analyzed and tested to determine the remaining risk of penetrating and lacerating injuries. Mitigations for laceration and penetration will be redesigned and retested if initial designs are not effective. Height-Velocity boundaries and/or operational procedures in the CONOP will be amended to show the impact KE levels defined by the FAA to achieve the defined target level of safety, or at a minimum the impact KE, defined by the applicant as safe for operations. Ranges of impact KE, as a function of altitude and velocity, will be defined by the applicant to provide a range of safe height-velocity profiles for the selected vehicle configuration. An example of height-velocity envelope development is shown in Appendix A – UAH Part 107 Waiver Submission for Flight Over People. The operational risk assessment (ORA) will be updated jointly by the applicant, representatives, and the FAA based on the results of testing an analysis in order to determine residual risk present in the CONOPS.

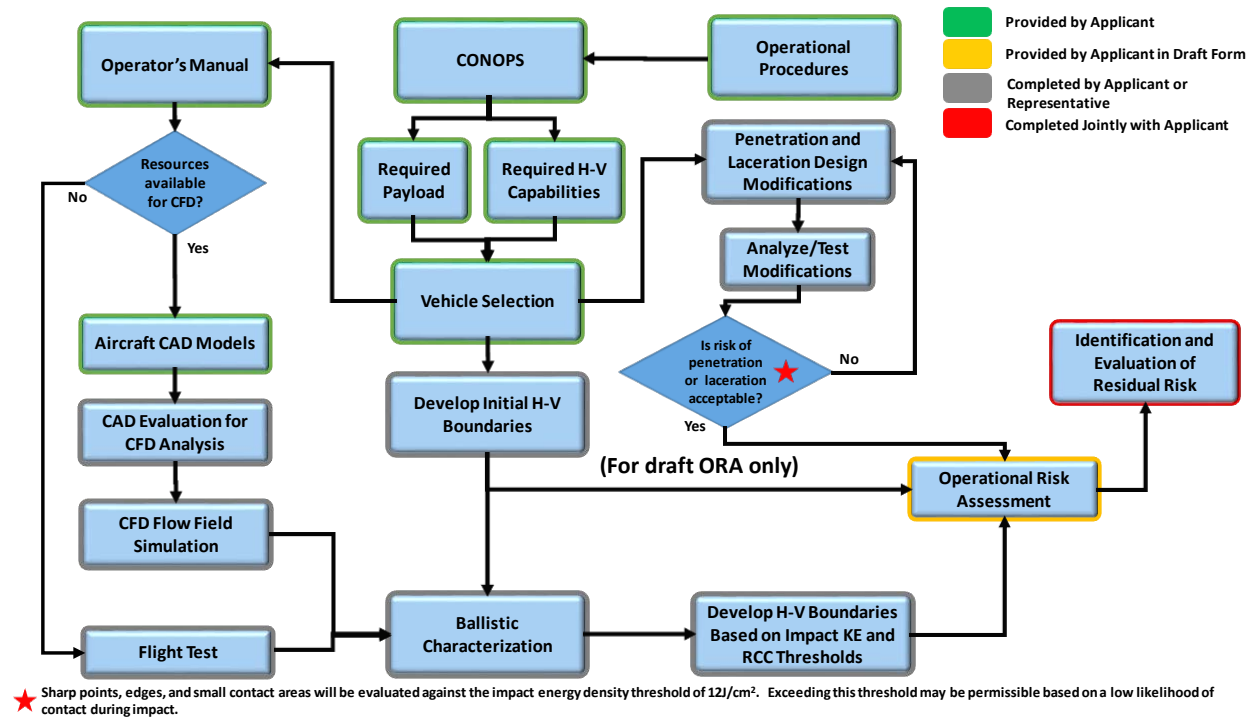


Figure C-1 - Testing and Analysis Standard Block Diagram

C.3. CONOPS Development

CONOPS development is the framework for the operational aspects of the mission that ultimately define the height-velocity operational restrictions. The development of the CONOPS is beyond the scope of this report, but the CONOPS should clearly articulate the operational requirements from which an operational risk assessment can be made. An example CONOPS is contained within the waiver in Appendix A. The CONOPS will take into account the applicant's existing operational procedures, which play a key role in the draft operational risk assessment and first set of risk mitigations developed under the waiver application.

Requirements within the CONOPS, in terms of payload capabilities and required height-velocity combinations drive vehicle selection by the applicant. Selection of the vehicle feeds three separate efforts within the testing and analysis. First, the vehicle's mass, along with assumed flat plate drag areas are used for an initial evaluation of Height-Velocity diagram which feeds development of the draft ORA. The selection also begins the process of developing injury mitigations for penetration and laceration injuries. Lastly, the vehicle selection feeds into ballistic characterization.

C.4. Ballistic Characterization Option 1: CFD Analysis of Flat Plate Drag Area

C.4.1. Development of CFD Models from Vehicle Computer-Aided Design (CAD) Models

A well-designed CAD model is critical for performing CFD and FEA simulations. There are several specific considerations when modeling for a CFD or FEA workflow. CAD models used for CFD are different than those used for manufacturing and those used for structural analysis. The CAD model must be watertight and free of discontinuous surfaces or gaps between intersecting surfaces. The amount of time to run a CFD or FEA simulation is a function of the size of the grid mesh applied over the surfaces. The grid size is determined by the area of the smallest face on the model; therefore, extremely small part faces or radius of curvature significantly increases the simulation run time. Selection of meaningful details that may impact drag calculations is critical in the development of the CFD model from CAD. Most industry CAD models require some modification from engineering and production drawings to conduct CFD analysis. A simpler method of refining flat plate drag for the vehicle can be conducted using a wetted area analysis if CFD cannot be conducted due to schedule or cost concerns.

For applicants who may not have access to the original aircraft manufacturer's CAD files, the applicant can use a coordinate measuring machine (CMM) to create point cloud data of the airframe which could then be translated through sketches to a solid CAD model. This method is a time consuming and expensive process in the absence of an expert who can perform this analysis. Many vehicles may have existing CAD available online that represent the vehicle with acceptable dimensional error. UAH used a CAD model of a Phantom 3 Advanced from GrabCAD that had acceptable dimensional accuracy for a baseline CAD model. Several

modifications were made to the downloaded CAD model to correct geometry errors and discontinuous surfaces to create a clean model to import the CFD workflow.

C.4.2. CFD Flow Field Simulation

The overarching goal of the CFD flow field simulation is to develop vertical and horizontal equivalent flat plate drag areas for a given vehicle. Equivalent flat plate drag is expressed as:

$$f = C_d A_{ref} \quad \text{Equation C - 1}$$

where C_d is the CFD-generated drag coefficient based on an assumed reference Area, or A_{ref} . The reference area is an assumed wetted area, because it is not possible to determine the actual wetted area for a complex shape, unlike an airfoil. Therefore, it must be emphasized that the calculated drag coefficients are specific to the assumed area and cannot be applied to other reference area values; however, the flat plate drag area is representative of the aircraft specifically.

It is recommended that the applicant utilize the vertical and horizontal projections of the vehicle viewed from above and the side, respectively as the reference areas such that the drag coefficient can be a reasonable value that makes engineering sense in the analysis. The A_{ref} values can be determined via CAD software or in a CFD environment. Standardized reference areas also assist in the calculation of the Reynolds number of the vehicle for simulation. The expression for Reynolds number is given by:

$$Re = \frac{\rho V L}{\mu} \quad \text{Equation C - 2}$$

where ρ is air density, V is the speed of incident flow, L is the characteristic length of the aircraft, and μ is dynamic viscosity. Given that sUAS, particularly multi-rotor sUAS, have widely varying geometries, it is challenging to develop a standard characteristic length based on vehicle arm length or fuselage length. The proposed method is to calculate the diameter of a circle with area equal to reference area of the vehicle. This diameter, in turn, is the characteristic length of the vehicle for flow coming from that direction. This means that there are different Re values for vertical and horizontal flow over the vehicle, even at the same incident flow velocity, because the characteristic length of the vehicle will generally be different when calculated based on vertical and horizontal projected areas. The relation for the characteristic length of the vehicle, for a given orientation with respect to flow, is given by:

$$L = 2 \sqrt{\frac{A_{eff}}{\pi}} \quad \text{Equation C - 3}$$

CFD modelers should complete grid sensitivity studies to ensure that grid densities are sufficient to estimate vehicle forces during simulation. Additionally, it is recommended that several turbulent flow models are used to compare estimated drag coefficients and provide several modeling options when correlating CFD and ballistic characterization results with flight test data during validation. The UAH modeling, which was validated for both the Phantom 2 and Phantom 3 aircraft, used laminar incident flow on the aircraft and a Turbulent Kinetic Energy method to model turbulent flow after separation from the fuselage and components. Both of these modeling methods appear to provide very accurate estimations of vehicle drag forces with estimated impact velocities being within 1% of observed impact velocities for most NIAR drop tests. The outlier cases, which replicated 40-foot drop tests, were within 2.2% (Appendix A – UAH Part 107 Waiver Submission for Flight Over People) of the observed velocities.

For standardization between analytical efforts, modelers will employ standard conditions, vehicle attitudes and incident flow velocities during CFD simulation. Standard Sea Level (SSL) air properties are recommended for use in CFD flow field simulation (Table C-1). CFD simulations must be completed for a range of speeds in orientations, with respect to flow, that represent vertical falling of the vehicle in a level attitude and horizontal flight in a level attitude. This is based on the assumption that the vehicle will fall in a level attitude. If designers know that a vehicle will fall in a different attitude, the simulation should be completed in orientations that reflect the known post-failure vehicle attitudes with respect to flow. The vehicle must have the same configuration during simulation as it will have during flight test and operational use, e.g. blade guards and with the appropriate payload(s) installed. The simulations will be completed for velocities that are representative of the vehicle’s minimum through maximum horizontal airspeeds and vertical speeds up through the terminal velocity of the aircraft.

Table C-1 - SSL Properties for CFD Analysis

Property	Pressure	Density	Viscosity
SI units	101.325 kPa	1.225 kg/m ³	1.789x10 ⁻⁵ Pa-s
English units	14.696 lbf/in ²	0.002377 slug/ft ³	3.737x10 ⁻⁷ slug/(s-ft)

The required minimum output of the flow field simulations are tables of vehicle drag coefficients and the respective effective areas of the vehicle based on orientation with respect to flow.

C.5. Flight Test Validation of Flat Plate Drag Area

C.5.1. Flight Test Requirements

Waiver applicants will complete flight testing in the proposed aircraft configuration, e.g. payload and blade guards etc., representative of how the aircraft will be flown under the waiver

CONOPS. This also applies to the use of a parachute recovery system if operators are planning to use a parachute for impact energy mitigation during waived operations.

Flight tests are aimed at collecting vehicle state data (velocities, attitudes, and angular rates) during a power-off descent. State will be collected using a data logger with a minimum of 5Hz sampling rate for vehicle state data. The required data outputs of the flight test are the vehicle pitch, roll, yaw, and vertical and horizontal velocity components with respect to time during fall for an unmitigated vehicle, i.e. without a parachute installed as part of the CONOP/waived operations. The ballistic characterization will be completed by comparing predicted and achieved vehicle trajectories (vertical and horizontal displacement of the vehicle as a function of time) during fall. This will be completed for a range of initial velocities at failure, e.g. 0, 5, 10, and 20 ft/s.

Testing to validate parachute recovery system performance must record the vehicle vertical and horizontal velocities after failure. It is desirable to log the parachute deployment signal to evaluate the time and altitude loss between when the parachute actuation command is transmitted to when the aircraft achieves a steady rate of descent under parachute. This will allow for determination of the minimum operating altitude required for operations with a parachute recovery system.

If ambient conditions during flight test vary more than 5 degrees Fahrenheit or 500 ft pressure altitude from the original ballistic characterization of the vehicle, then the characterization of the vehicle should be rerun under the same conditions as the flight test.

C.6. Ballistic Characterization Option 2: Determine Flat Plate Drag and Ballistics by Flight Test Only

Operators may conduct flight test only, in lieu of CFD simulation, to support ballistic characterization, based on limited available time, funding, CFD software and CFD modeling expertise. This flight test is meant to replicate ballistic characterization, albeit at a lower level of fidelity in terms of the number of failure altitude and airspeeds that are tested. This means that the testing must also verify the vehicle's terminal velocity following failure. Any fall altitude that is sufficient to achieve terminal velocity covers the need for variation in failure altitude. Failure airspeeds, during flight test, must be representative of the range of operating airspeeds for the planned operations under waiver. There may be minor fluctuations in the recorded terminal velocity values during a drop test, because of wake shedding and resulting changes in pressure drag. An average value may be taken to be the vehicle's stabilized or quasi-static terminal velocity. The vehicle terminal velocity will be used to calculate the worst case impact KE value and the vehicle's flat plate drag area at terminal velocity. The flat plate drag area will be calculated as follows:

$$f = A_{eff} C_d = \frac{2mg}{\rho V_{terminal}^2} \quad \text{Equation C - 4}$$

where g is the rate of gravitational acceleration and ρ is the density of the ambient air during flight testing.

C.7. Instrumentation and Data Collection Requirements

Table C-2 shows the minimum required vehicle state data needed for validation of ballistic models. The minimum required sampling rate for all vehicle parameters is 5Hz. All parameters must have time stamps in order to determine the total velocity and attitude of the aircraft at any point in time during a drop. The pitch, roll, and yaw parameters are recorded to verify the vehicle attitude during drop – one key aspect of validating the ballistic model is to verify that the vehicle falls, while unpowered, with the same attitude that was assumed during CFD flat-plate drag area estimation and ballistic characterization. There will be discrepancies between the predicted and observed descent and drift rates if the actual falling attitude is different than the falling attitude that was modeled. As such, the flight test will not serve as validation because the model is inaccurate.

Table C-2 - Flight Test Instrumentation Requirements

Parameter	Minimum Sampling Rate	Remarks
Time	5 Hz	
Altitude	5 Hz	Must be timestamped
V _z	5 Hz	Must be timestamped
V _x	5 Hz	Must be timestamped
V _y	5 Hz	Must be timestamped
Roll	5 Hz	Must be timestamped
Pitch	5 Hz	Must be timestamped
Yaw	5 Hz	Must be timestamped

The terminal velocity, which can generally be reached in approximately 200 ft of falling for a multi-rotor aircraft, is used to calculate the effective flat plate drag of the vehicle. Operators will have to conduct several vertical drop tests to ensure consistency and verification of the terminal velocity value. Flat plate drag area is calculated, from terminal velocity, by the following relationship:

$$f = \frac{2mg}{\rho V_{term}^2} \quad \text{Equation C - 5}$$

Flight test data will be post-processed in order to determine the vehicle's vertical and lateral displacement based on time. The ballistic modeling will be validated by comparing the predicted vehicle trajectory for a given failure flight condition, in terms of failure horizontal velocity and altitude, with the observed trajectory from flight test. The flight test trajectory can be developed directly from altitude and drift recorded by the data logger or calculated based on the vehicle's

instantaneous velocity at each time step and the interval between time steps. The vertical displacement at any time step, based on the latter method, is calculated by:

$$z = z_i + V_z \Delta t \quad \text{Equation C - 6}$$

where z_i is the initial altitude and Δt is the interval between altitude samples in the data logger. The horizontal displacement is calculated at any time step by:

$$x = x_i + V_h \Delta t \quad \text{Equation C - 7}$$

where V_h is the resultant velocity vector based on the vehicle's x and y velocities during the fall. In this analysis, the point where motor power is cut off is treated as $x = 0$. Figure 1 provides an example of comparing predicted and actual post-failure trajectories.

C.8. Vehicle Ballistic Analysis/Characterization

The vehicle ballistic characterization provides estimated impact KE values for the UAS based on combinations of failure altitude and airspeed. The characterization also provides estimated impact angles for the aircraft. Examples of these outputs are provided in Figures C – 5, C – 6, C – 19, and C – 20 in Appendix A – UAH Part 107 Waiver Submission for Flight Over People. This is purely a ballistic modeling effort that assumes a constant vehicle attitude during descent, full loss of propulsion, and failure in a level attitude with no representation of vehicle dynamics. It represents a failure scenario in which the vehicle falls as an inert mass. Basic characterization of the vehicle should be conducted to produce impact KE values based on failure under SSL conditions. If operators expect to conduct operations under unique conditions, i.e. high and hot conditions, the simulation inputs should represent those conditions to determine worst case impact KE values. The failure altitude and velocity combinations used in the ballistic characterization should reflect the operators full desired operating envelope, which will be related to the accompanying waiver CONOPS.

C.9. Injury Mitigations

Waiver applicants must develop, validate, and apply mitigations to all identifiable categories of human injury that can result from malfunction of their aircraft during missions conducted under a waiver to Part 107 operating restrictions. The known injury types inherent to sUAS collision with a person, per the Project A4 White Paper on UAS Characteristics are blunt trauma, penetrating injuries, and laceration injuries. Mitigations can be in the form of operational restrictions, e.g. operating height-velocity limits to minimize impact energy, or design modifications like shrouds, guards, or padding to minimize the most likely means of causing penetration or laceration injuries, or any other means that an applicant can devise.

Waiver applications will contain data and analysis that validates the effectiveness of applied mitigations and the correctness of any engineering assumptions, for example, assumed energy transfer values during sUAS collision with a person. Validation may take the form of safety case

analysis based on the CONOPS and flight test data and/or ballistic modeling. It can also come from experimental work, for example impact testing of blade guards to measure resilience and determine residual injury risk. All analytical modeling efforts require some form of experimental validation. Design mitigations and operational limits will be tested and revised, as needed, until appropriate levels of safety are reached based on ground impact KE levels. It is important to emphasize that data from experiments and modeling should provide the FAA with an understanding of the residual risk after the mitigation is applied. Information about the residual risk feeds both the waiver applicant's Operational Risk Assessment process and document, and allows the FAA to make clear determinations of acceptable operations and mitigations on a case-by-case basis. The absence of identified residual risk will likely hinder FAA evaluation of the waiver package.

C.9.1. Blunt Trauma Injuries

The assessment of blunt trauma injury potential and PoF will be conducted by comparing predicted and observed ground impact KE values from ballistic characterization with RCC thresholds. Blunt trauma PoF values can be determined using values shown in Figure 7 or Figure 8 depending on the application and the knowledge of whether non-participants are sitting, standing or laying down as defined in the CONOPS.

C.9.2. Penetrating Injuries

Penetration injuries can be assessed against impact KEs and the contact areas that may result during collision events to identify local areas of focused energy. Energy densities of components that exceed 57 ft-lbs/in² (12 lbs/cm²) should be addressed to reduce injury potential. These values should not be used as reasons for rejecting the applicant's request. Landing gear, payloads and blade guards are potential sources of penetrating injuries. Landing gear and blade guards are typically flexible and absorb energy that reduce energy density when compared with straight calculations of impact energy divided by the contact areas. Payloads typically have frangible fittings or mounts that cause the payload to break away under load or absorb some of the energy and reduce the energy density during collision. For these reasons, the energy density standards cannot be applied as a rigid test, but analyzed to determine how sufficiently the mitigation has reduced the hazard relative to the impact energies and the collision orientations identified by the applicant.

C.9.3. Laceration Injuries

Laceration injuries are the result of blade contact with unprotected skin. Even light clothing can mitigate laceration injuries to some degree. Multiple blade contacts with unprotected skin and deep penetration injuries greater than ½ inch cause the most severe injuries. Small lacerations to the head can cause more substantial bleeding, while lacerations to the neck area are the most severe especially when the carotid artery is involved. Laceration injuries that result in injuries of AIS3 or greater involve more than 20% loss of blood by volume or involve bilateral lacerations

to arteries such as the carotid artery during a single collision. Blade guards create the simplest and most effective form of mitigation to laceration injuries when the blade guards are capable of sustaining impacts at the impact velocities identified within the height-velocity diagrams without allowing only momentary penetration into the cutting area by less than ½ inch before rebounding the vehicle away from the person. Blade guards also create collision geometries with other parts of the vehicle that prevent the vehicle from reaching small areas such as the neck when descending at steep angles. For flight over people waivers, the applicant should show how the blade guards function under collision velocities to minimize intrusion into the cutting area by less than ½ in. as long as they rebound the vehicle away from the person. Furthermore, blade guards may be designed to intrude into the blade area causing blade stoppage during the collision, and the applicant should show how the blade guards operate at a variety of impact angles and collision velocities within the operating envelope. The applicant should also show how blade guards may mitigate access to the thorax/neck area, as these areas are the most vulnerable to laceration injuries. These mitigations are deemed as acceptable since they mitigate the majority of AIS 3 or greater laceration injuries that blades can induce following a collision. Blade guards will always be limited in performance due to weight and drag. As such, failure of the blade guards during testing should not be a reason for rejecting the mitigation as long as the vehicle rebounds away from the person during the collision when the blade guard fails. Blade guards should survive multiple contacts when the CONOPS requires flight over a densely populated operation over people, and there are no other mitigations for blade stoppage following the first collision since the vehicle can rebound from one individual and contact another under these type scenarios.

C.10. Operational Risk Assessment (ORA)

The operational risk assessment is beyond the scope of this report, but the operational risk assessment should define the failure scenarios, associated severity of the hazard resulting from the failure and the appropriate mitigations used to mitigate the hazard. Of particular importance for this effort is for the applicant to review the vehicle configuration for potential blunt force trauma, penetration injuries and laceration injuries that this vehicle configuration might cause during a collision scenario with a non-participant or a participant for that matter. Blunt force trauma is related to the impact KE and mitigations are related to how the impact KE is reduced prior to collision or during the collision due to absorption by the vehicle or frangibility of the vehicle. Penetration injuries are focused on sharp edges of the vehicle other than rotating components or small contact areas where the impact KE may become concentrated in a single area. Laceration injuries are related to impacts by rotating blades caused by rotors or propellers. These laceration injuries are isolated from lacerations that might occur from penetration injuries of non-rotating components since their mitigations are uniquely different.

The identification of these mitigations are important to identify early as many of the proposed mitigations can have an impact on flat plate drag area and the ultimate vehicle configuration.

An example ORA is contained in the waiver request contained in Appendix A. More research is required to develop a comprehensive ORA for UAS operations in general so one is not provided as part of this report. Many of the hazards identified in the ORA contained in Appendix A are common hazards to most UAS operations and may support the development of future ORAs until a comprehensive example can be developed. The ASSURE Team has proposed developing a comprehensive ORA outline for UAS operations.

The applicant will coordinate with the FAA to reach consensus on the level of residual risk inherent to the operations covered by the waiver application.

Appendix D - Proposed Standard with Evaluation of Potential Injury Severity

D.1. Introduction

The tests and analysis conducted under Task A4 and Task A11 of the FAA UAS CoE have led to the development of a proposed standard to be used by industry to substantiate vehicle-specific operational height-velocity envelopes for safe operation for flight over people. The proposed standard uses the same methodology used to establish an envelope during Task A11.

Additionally, the standard outlines test procedures that can be conducted by the applicant that do not require use of a separate testing site or significant increase in costs or time to collect envelope validation data for part 107 waiver submission. This standard also develops new procedures for assessing injury metrics without using RCC metrics for impact PoF only. The basic steps in the process are as follows:

- a. Develop a CONOPS.
- b. Conduct an operational safety assessment to identify hazards.
- c. Identify aircraft modifications required for mitigations for laceration and penetration injury hazards (parachutes, blade guards, material selection, frangibility, etc.).
- d. Conduct CFD analysis or other analysis to determine the flat plate drag area and mass of the applicant's proposed vehicle configuration to refine the height-velocity diagram.
- e. Conduct a ballistic analysis/characterization of the applicant vehicle based upon flat plate drag area and mass of the applicant's proposed vehicle configuration to develop initial height-velocity diagram to achieve CONOPS.
- f. Conduct flight test to substantiate the flat plate drag area and mass of the applicant's proposed vehicle configuration to refine the height-velocity diagram from the original ballistic analysis.
- g. Analyze resultant impact loads based upon mass and velocity of the vehicle at the corner points of the height-velocity diagram to determine AIS injury standard does not exceed 30% chance of AIS 3 or greater injury for head and neck injuries (limiting factor). All areas of the height-velocity diagram must not exceed 30% probability of resulting in an AIS 3 or greater injury.

D.2. Flow chart with Data Requirements

The data requirements to support this testing standard and the testing standard workflow are illustrated in Figure D-1. The applicant must provide aircraft CAD models, the CONOPS describing the operations covered by the waiver application, and the vehicle model. An initial operational safety assessment will be provided by the applicant. Depending on the availability of

time, funding, software and expertise, an applicant may choose to conduct ballistic characterization via CFD flow field simulation, ballistic modeling, and flight test validation, or conduct an in-depth flight test to support ballistic characterization. In the former method, the applicant or a representative organization will evaluate and modify aircraft CAD models for use in CFD simulation and then conduct ballistic characterization of the vehicle based on the vehicle mass and aerodynamic properties. The applicant or a representative will conduct flight test following integration of the vehicle state data logging unit and procedures are established for safe recovery of the vehicle following power-off drops from altitude. If an applicant chooses to use flight test alone, this will be used to verify the vertical flat plate drag area of the vehicle and impact KE-levels based on failure airspeed. The applicant or a representative will conduct resultant impact load analysis and injury severity correlation based on achieved impact KE values, and develop mitigations for penetration and laceration injuries. Penetration and laceration mitigations will be analyzed and tested to determine the remaining risk of penetrating and lacerating injuries. Mitigations for laceration and penetration will be redesigned and retested if initial designs are not effective. If resultant impact load and correlated blunt trauma injury severity estimates exceed 30% probability of an AIS-3 or greater injury, the Height-Velocity Boundaries in the CONOP will be amended or operational procedures will be amended until accepted injury severity levels are reached. The operational risk assessment (ORA) will be updated jointly by the applicant, representatives, and the FAA based on the results of testing an analysis in order to determine residual risk present in the CONOPS.

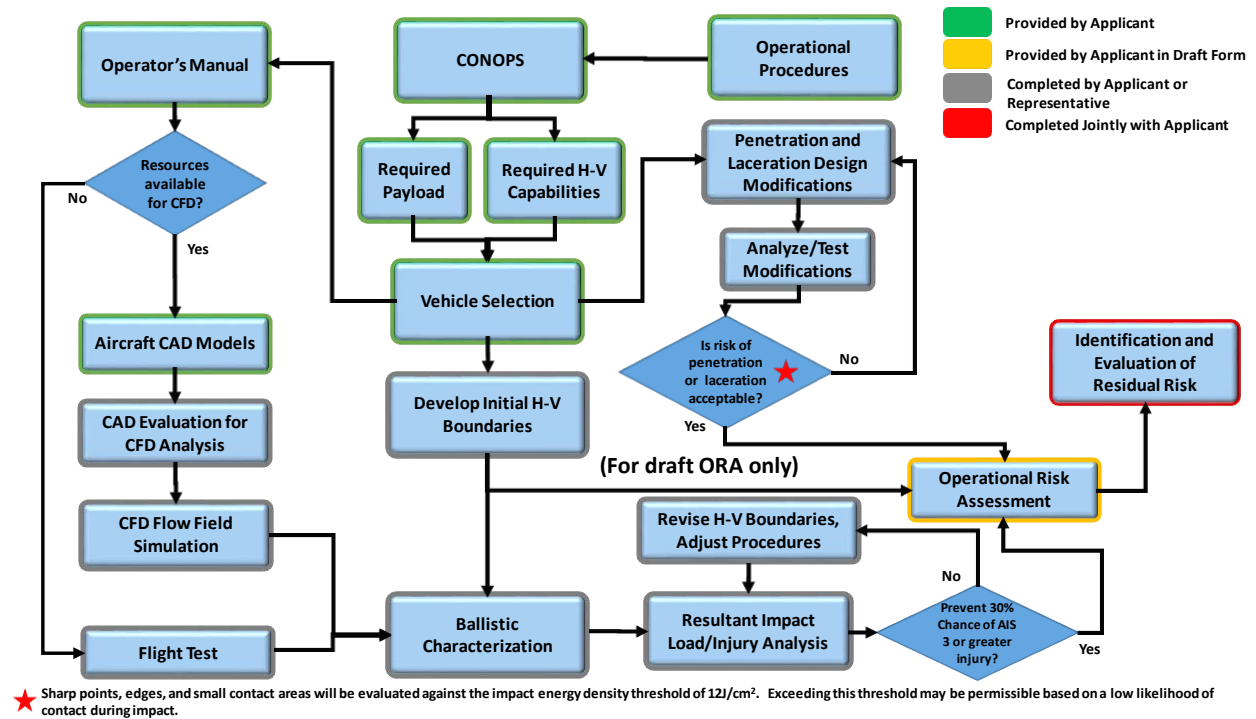


Figure D-1 - Testing and Analysis Flow Chart and Data Input Requirements

D.3. CONOPS Development

CONOPS development is the framework for the operational aspects of the mission that ultimately the height-velocity operational restrictions are defined. The development of the CONOPS is beyond the scope of this report, but the CONOPS should clearly articulate the operational requirements from which an operational risk assessment can be made. The outline for a CONOPS is contained in Appendix B, and an example CONOPS is contained within the waiver in Appendix A. The CONOPS will take into account the applicant's existing operational procedures, which play a key role in the draft operational risk assessment and first set of risk mitigations developed under the waiver application.

Requirements within the CONOPS, in terms of payload capabilities and required height-velocity combinations, drive vehicle selection by the applicant. Selection of the vehicle feeds three separate efforts within the testing and analysis. First, the vehicle's mass, along with assumed flat plate drag areas are used for an initial evaluation of Height-Velocity diagram which feeds development of the draft ORA. The selection also begins the process of developing injury mitigations for penetration and laceration injuries. Lastly, the vehicle selection feeds into ballistic characterization.

D.4. Ballistic Characterization Option 1: CFD Analysis of Flat Plate Drag Area

D.4.1. Development of CFD Models from Vehicle Computer-Aided Design (CAD) Models

A well-designed CAD model is critical for performing CFD and FEA simulations. There are several specific considerations when modeling for a CFD or FEA workflow. CAD models used for CFD are different than those used for manufacturing and those used for structural analysis. The CAD model must be watertight and free of discontinuous surfaces or gaps between intersecting surfaces. The amount of time to run a CFD or FEA simulation is a function of the size of the grid mesh applied over the surfaces. The grid size is determined by the area of the smallest face on the model; therefore, extremely small part faces or radius of curvature significantly increase the simulation run time and selection of meaningful detail that may impact drag calculations is critical in the development of the CFD model from CAD. Most industry CAD models require some modification from engineering and production drawings to conduct CFD analysis. A simpler method of refining flat plate drag for the vehicle can be conducted using a wetted area analysis if CFD cannot be conducted due to schedule or cost concerns.

For applicants who may not have access to the original aircraft manufacturer's CAD files, the applicant can use a coordinate measuring machine (CMM) to create point cloud data of the airframe which could then be translated through sketches to a solid CAD model. This method is a time consuming and expensive process in the absence of an expert who can perform this

analysis. Many vehicles may have existing CAD available online that represent the vehicle with acceptable dimensional error. UAH used a CAD model of a Phantom 3 Advanced from GrabCAD that had acceptable dimensional accuracy for a baseline CAD model. Several modifications were made to the downloaded CAD model to correct geometry errors and discontinuous surfaces to create a clean model to import the CFD workflow.

D.4.2. CFD Flow Field Simulation

The overarching goal of the CFD flow field simulation is to develop vertical and horizontal equivalent flat plate drag areas for a given vehicle. Equivalent flat plate drag is expressed as:

$$f = C_d A_{ref} \quad \text{Equation D - 1}$$

where C_d is the CFD-generated drag coefficient based on an assumed reference Area or A_{ref} . The reference area is an assumed wetted area, because it is not possible to determine the actual wetted area for a complex shape, unlike an airfoil. Therefore, it must be emphasized that the calculated drag coefficients are specific to the assumed area and cannot be applied to other reference area values; however, the flat plate drag area is representative of the aircraft specifically.

It is recommended that the applicant utilizes the vertical and horizontal projections of the vehicle then viewed from above and the side, respectively as the reference area such that the drag coefficient can be a reasonable value that makes engineering sense in the analysis. The A_{ref} values can be determined via CAD software or in a CFD environment. Standardized reference areas also assist in the calculation of the Reynolds number of the vehicle for simulation. The expression for Reynolds number is given by:

$$Re = \frac{\rho V L}{\mu} \quad \text{Equation D - 2}$$

where ρ is air density, V is the speed of incident flow, L is the characteristic length of the aircraft, and μ is dynamic viscosity. Given that sUAS, particularly multi-rotor sUAS, have widely varying geometries, it is challenging to develop a standard characteristic length based on vehicle arm length or fuselage length. The proposed method is to calculate the diameter of a circle with area equal to the reference area of the vehicle. This diameter, in turn, is the characteristic length of the vehicle for flow coming from that direction. This means that there are different Re values for vertical and horizontal flow over the vehicle, even at the same incident flow velocity, because the characteristic length of the vehicle will, generally, be different when calculated based on vertical and horizontal projected areas. The relation for the characteristic length of the vehicle, for a given orientation with respect to flow, is given by:

$$L = 2 \sqrt{\frac{A_{eff}}{\pi}} \quad \text{Equation D - 3}$$

CFD modelers should complete grid sensitivity studies to ensure that grid densities are sufficient to estimate vehicle forces during simulation. Additionally, it is recommended that several turbulent flow models are used to compare estimated drag coefficients and provide several modeling options when correlating CFD and ballistic characterization results with flight test data during validation. The UAH modeling, which was validated for both the Phantom 2 and Phantom 3 aircraft, used laminar incident flow on the aircraft and a Turbulent Kinetic Energy method to model turbulent flow after separation from the fuselage and components. Both of these modeling methods appear to provide a very accurate estimation of vehicle drag forces with estimated impact velocities being within 1% of observed impact velocities for most NIAR drop tests. The outlier cases, which replicated 40-foot drop tests, were within 2.2% (Appendix A – UAH Part 107 Waiver Submission for Flight Over People) of the observed velocities.

For standardization between analytical efforts, modelers will employ standard conditions, vehicle attitudes and incident flow velocities during CFD simulation. Standard Sea Level (SSL) air properties are recommended for use in CFD flow field simulation (Table D-1). CFD simulations must be completed for a range of speeds in orientations, with respect to flow, that represent vertical falling of the vehicle in a level attitude and horizontal flight in a level attitude. This is based on the assumption that the vehicle will fall in a level attitude. If designers know that a vehicle will fall in a different attitude, the simulation should be completed in orientations that reflect the known post-failure vehicle attitudes with respect to flow. The vehicle must have the same configuration during simulation as it will have during flight test and operational use, e.g. blade guards and with the appropriate payload(s) installed. The simulations will be completed for velocities that are representative of the vehicle’s minimum through maximum horizontal airspeeds and vertical speeds up through the terminal velocity of the aircraft.

Table D-1 - SSL Air Properties for CFD Analysis

Property	Pressure	Density	Viscosity
SI units	101.325 kPa	1.225 kg/m ³	1.789x10 ⁻⁵ Pa-s
English units	14.696 lbf/in ²	0.002377 slug/ft ³	3.737x10 ⁻⁷ slug/(s-ft)

The required minimum output of the flow field simulations are tables of vehicle drag coefficients and the respective effective areas of the vehicle based on orientation with respect to flow.

D.5. Flight Test Validation of Flat Plate Drag Area

D.5.1. Flight Test Requirements

Waiver applicants will complete flight testing in the proposed aircraft configuration, e.g. payload and blade guards, etc., representative of how the aircraft will be flown under the waiver CONOPS. This also applies to the use of a parachute recovery system if operators are planning to use a parachute for impact energy mitigation during waived operations.

Flight tests are aimed at collecting vehicle state data (velocities, attitudes, and angular rates) during a power-off descent. State will be collected using a data logger with a minimum of 5Hz sampling rate for vehicle state data. The required data outputs of the flight test are the vehicle pitch, roll, yaw, and vertical and horizontal velocity components with respect to time during fall for an unmitigated vehicle, i.e. without a parachute installed as part of the CONOP/waivered operations. The ballistic characterization will be completed by comparing predicted and achieved vehicle trajectories (vertical and horizontal displacement of the vehicle as a function of time) during fall. This will be completed for a range of initial velocities at failure, e.g. 0, 5, 10, and 20 ft/s.

Testing to validate parachute recovery system performance must record the vehicle vertical and horizontal velocities after failure. It is desirable to log the parachute deployment signal to evaluate the time and altitude loss between when the parachute actuation command is transmitted to when the aircraft achieves a steady rate of descent under parachute. This will allow for determination of the minimum operating altitude required for operations with a parachute recovery system.

If ambient conditions during flight test vary more than 5 degrees Fahrenheit or 500 ft pressure altitude from the original ballistic characterization of the vehicle, then the characterization of the vehicle should be rerun under the same conditions as the flight test.

D.5.2. Ballistic Characterization Option 2: Determine Flat Plate Drag and Ballistics by Flight Test Only

Operators may conduct flight test only, in lieu of CFD simulation, to support ballistic characterization, based on limited available time, funding, CFD software and CFD modeling expertise. This flight test is meant to replicate ballistic characterization, albeit at a lower level of fidelity in terms of the number of failure altitude and airspeeds that are tested. This means that the testing must also verify the vehicle's terminal velocity following failure. Any fall altitude that is sufficient to achieve terminal velocity covers the need for variation in failure altitude. Failure airspeeds, during flight test, must be representative of the range of operating airspeeds for the planned operations under waiver. There may be minor fluctuations in the recorded terminal velocity values during a drop test, because of wake shedding and resulting changes in pressure drag. An average value may be taken to be the vehicle's stabilized or quasi-static terminal velocity. The vehicle terminal velocity will be used to calculate the worst case impact KE value and the vehicle's flat plate drag area at terminal velocity. The flat plate drag area will be calculated as follows:

$$f = A_{eff}C_d = \frac{2mg}{\rho V_{terminal}^2} \quad \text{Equation D - 4}$$

where g is the rate of gravitational acceleration and ρ is the density of the ambient air during flight testing.

D.5.3. Instrumentation and Data Collection Requirements

Table D-2 shows the minimum required vehicle state data needed for validation of ballistic models. The minimum required sampling rate for all vehicle parameters is 5Hz. All parameters must have timestamps in order to determine the total velocity and attitude of the aircraft at any point in time during a drop. The pitch, roll, and yaw parameters are recorded to verify the vehicle attitude during drop – one key aspect of validating the ballistic model is to verify that the vehicle falls, while unpowered, with the same attitude that was assumed during CFD flat-plate drag area estimation and ballistic characterization. There will be discrepancies between the predicted and observed descent and drift rates if the actual falling attitude is different than the falling attitude that was modeled. As such, the flight test will not serve as validation, because the model is inaccurate.

Table D-2 - Flight Test Instrumentation Requirements

Parameter	Minimum Sampling Rate	Remarks
Time	5 Hz	
Altitude	5 Hz	Must be timestamped
V _z	5 Hz	Must be timestamped
V _x	5 Hz	Must be timestamped
V _y	5 Hz	Must be timestamped
Roll	5 Hz	Must be timestamped
Pitch	5 Hz	Must be timestamped
Yaw	5 Hz	Must be timestamped

The terminal velocity, which can generally be reached in approximately 200 ft of falling for a multi-rotor aircraft, is used to calculate the effective flat plate drag of the vehicle. Operators will have to conduct several vertical drop tests to ensure consistency and verification of the terminal velocity value. Flat plate drag area is calculated, from terminal velocity, by the following relationship:

$$f = \frac{2mg}{\rho V_{term}^2} \quad \text{Equation D - 5}$$

Flight test data will be post-processed in order to determine the vehicle's vertical and lateral displacement based on time. The ballistic modeling will be validated by comparing the predicted vehicle trajectory for a given failure flight condition, in terms of failure horizontal velocity and altitude, with the observed trajectory from flight test. The flight test trajectory can be developed directly from altitude and drift recorded by the data logger or calculated based on the vehicle's instantaneous velocity at each time step and the interval between time steps. The vertical displacement at any time step, based on the latter method, is calculated by:

$$z = z_i + V_z \Delta t \quad \text{Equation D - 6}$$

where z_i is the initial altitude and Δt is the interval between altitude samples in the data logger. The horizontal displacement is calculated at any time step by:

$$x = x_i + V_h \Delta t \quad \text{Equation D - 7}$$

where V_h is the resultant velocity vector based on the vehicle's x and y velocities during the fall. In this analysis, the point where motor power is cut off is treated as $x = 0$. Figure 1 provides an example of comparing predicted and actual post-failure trajectories.

D.6. Vehicle Ballistic Analysis/Characterization

The vehicle ballistic characterization provides estimated impact KE values for the UAS based on combinations of failure altitude and airspeed. The characterization also provides estimated impact angles for the aircraft. Examples of these outputs are provided in Figures C – 5, C – 6, C – 19, and C – 20 in Appendix A – UAH Part 107 Waiver Submission for Flight Over People. This is purely a ballistic modeling effort that assumes a constant vehicle attitude during descent, full loss of propulsion, and failure in a level attitude with no representation of vehicle dynamics. It represents a failure scenario in which the vehicle falls as an inert mass. Basic characterization of the vehicle should be conducted to produce impact KE values based on failure under SSL conditions. If operators expect to conduct operations under unique conditions, i.e. high and hot conditions, the simulation inputs should represent those conditions to determine worst case impact KE values. The failure altitude and velocity combinations used in the ballistic characterization should reflect the operators full desired operating envelope, which will be related to the accompanying waiver CONOPS.

D.7. Injury Mitigations

Waiver applicants must develop, validate, and apply mitigations to all identifiable categories of human injury that can result from malfunction of their aircraft during missions conducted under a waiver to Part 107 operating restrictions. The known injury types inherent to sUAS collision with a person, per the Project A4 White Paper on UAS Characteristics are blunt trauma, penetrating injuries, and laceration injuries. Mitigations can be in the form of operational restrictions, e.g. operating height-velocity limits to minimize impact energy, or design modifications like shrouds, guards, or padding to minimize the most likely means of causing penetration or laceration injuries, or any other means that an applicant can devise.

Waiver applications will contain data and analysis that validates the effectiveness of applied mitigations and the correctness of any engineering assumptions, for example, assumed energy transfer values during sUAS collision with a person. Validation may take the form of safety case analysis based on the CONOPS and flight test data and/or ballistic modeling. It can also come from experimental work, for example, impact testing of blade guards to measure resilience and determine residual injury risk. All analytical modeling efforts require some form of experimental validation. Design mitigations and operational limits will be tested and revised, as

needed, until appropriate levels of safety are reached, e.g. reducing blunt trauma injury severity to a 30% or less than of AIS-3 or greater severity of injury. It is important to emphasize that data from experiments and modeling should provide the FAA with an understanding of the residual risk after the mitigation is applied. Information about the residual risk feeds both the waiver applicant's Operational Risk Assessment process and document and allows the FAA to make clear determinations of acceptable operations and mitigations on a case-by-case basis. The absence of identified residual risk will likely hinder FAA evaluation of the waiver package.

D.8. Injury Analysis

D.8.1. Blunt Trauma Injuries

The applicant would determine the resultant load for head and neck injuries using the following equation.

$$\text{Resultant Load Factor (g)} = 1.5441 * \text{impact KE (ft - lbs)} \quad \text{Equation D - 8}$$

The impact KE is derived from the ballistic analysis for the vehicle configuration under evaluation, and the resultant load factor is calculated. As long as the resultant load factor remains below 196 g, then there is a 98% confidence that no skull fractures will occur and there will be less than 30% probability of having a neck injury exceed AIS3 or greater. The limit of this analysis is for multi-rotor vehicles made with plastic, flexible structures. The analysis applies to blunt force trauma type injuries. Laceration and penetration injuries must be addressed separately.

D.8.2. Penetrating Injuries

Penetration injuries can be assessed against impact KEs and the contact areas that may result during collision events to identify local areas of focused energy. Energy densities of components that exceed 57 ft-lbs/in² (12 lbs/cm²) should be addressed to reduce injury potential. These values should not be used as reasons for rejecting the applicant's request. Landing gear, payloads and blade guards are potential sources of penetrating injuries. Landing gear and blade guards are typically flexible and absorb energy that reduce energy density when compared with straight calculations of impact energy divided by the contact areas. Payloads typically have frangible fittings or mounts that cause the payload to break away under load or absorb some of the energy and reduce the energy density during collision. For these reasons, the energy density standards cannot be applied as a rigid test, but analyzed to determine how sufficiently the mitigation has reduced the hazard relative to the impact energies and the collision orientations identified by the applicant.

D.8.3. Laceration Injuries

Laceration injuries are the result of blade contact with unprotected skin. Even light clothing can mitigate laceration injuries to some degree. Multiple blade contacts with unprotected skin and

deep penetration injuries greater than ½ inch cause the most severe injuries. Small lacerations to the head can cause more substantial bleeding while lacerations to the neck area are the most severe especially when the carotid artery is involved. Laceration injuries that result in injuries of AIS3 or greater involve more than 20% loss of blood by volume or involve bilateral lacerations to arteries such as the carotid artery during a single collision. Blade guards create the simplest and most effective form of mitigation to laceration injuries when the blade guards are capable of sustaining impacts at the impact velocities identified within the height-velocity diagrams without allowing only momentary penetration into the cutting area by less than ½ inch before rebounding the vehicle away from the person. Blade guards also create collision geometries with other parts of the vehicle that prevent the vehicle from reaching small areas such as the neck when descending at steep angles. For flight over people waivers, the applicant should show how the blade guards function under collision velocities to minimize intrusion into the cutting area by less than ½ in as long as they rebound the vehicle away from the person. Furthermore, blade guards may be designed to intrude into the blade area causing blade stoppage during the collision, and the applicant should show how the blade guards operate at a variety of impact angles and collision velocities within the operating envelope. The applicant should also show how blade guards may mitigate access to the thorax/neck area as these areas are the most vulnerable to laceration injuries. These mitigations are deemed as acceptable since they mitigate the majority of AIS 3 or greater laceration injuries that blades can induce following a collision. Blade guards will always be limited in performance due to weight and drag. As such, failure of the blade guards during testing should not be a reason for rejecting the mitigation as long as the vehicle rebounds away from the person during the collision when the blade guard fails. Blade guards should survive multiple contacts when the CONOPS requires flight over a densely populated operation over people and there are no other mitigations for blade stoppage following the first collision since the vehicle can rebound from one individual and contact another under these type scenarios.

D.9. Operational Risk Assessment (ORA)

The operational risk assessment is beyond the scope of this report, but the operational risk assessment should define the failure scenarios, associated severity of the hazard resulting from the failure and the appropriate mitigations used to mitigate the hazard. Of particular importance for this effort is for the applicant to review the vehicle configuration for potential blunt force trauma, penetration injuries and laceration injuries that this vehicle configuration might cause during a collision scenario with a non-participant or a participant for that matter. Blunt force trauma is related to the impact KE, and mitigations are related to how the impact KE is reduced prior to collision or during the collision due to absorption by the vehicle or frangibility of the vehicle. Penetration injuries are focused on sharp edges of the vehicle other than rotating components or small contact areas where the impact KE may become concentrated in a single area. Laceration injuries are related to impacts by rotating blades caused by rotors or propellers.

These laceration injuries are isolated from lacerations that might occur from penetration injuries of non-rotating components since their mitigations are uniquely different.

The identification of these mitigations are important to identify early as many of the proposed mitigations can have an impact on flat plate drag area and the ultimate vehicle configuration.

An example ORA is contained in the waiver request contained in Appendix A. More research is required to develop a comprehensive ORA for UAS operations in general so one is not provided as part of this report. Many of the hazards identified in the ORA contained in Appendix A are common hazards to most UAS operations and may support the development of future ORAs until a comprehensive example can be developed. The ASSURE Team has proposed developing a comprehensive ORA outline for UAS operations.

The applicant will coordinate with the FAA to reach consensus on the level of residual risk inherent to the operations covered by the waiver application.